AWARD NUMBER: W81XWH-16-1-0474

TITLE: An Association of Unique microRNA Turnover Machinery with Prostate Cancer Progression

PRINCIPAL INVESTIGATOR: Hsieh, Jer-Tsong

CONTRACTING ORGANIZATION: University of Texas Southwestern Medical Center
Dallas, TX 75390

REPORT DATE: October 2017

TYPE OF REPORT: Annual

PREPARED FOR: U.S. Army Medical Research and Materiel Command
Fort Detrick, Maryland 21702-5012

REPORT DOCUMENTATION PAGE

Form Approved
OMB No. 0704-0188

1. REPORT DATE	2. REPORT TYPE	3. DATES COVERED
October 2017	Annual	15 Sep 2016 - 14 Sep 2017

4. Title
An Association of Unique microRNA Turnover Machinery with Prostate Cancer Progression

5a. CONTRACT NUMBER

5b. GRANT NUMBER
W81XWH-16-1-0474

5c. PROGRAM ELEMENT NUMBER

6. AUTHOR(S)
Jer-Tsong Hsieh

E-Mail: jt.hsieh@utsouthwestern.edu

5d. PROJECT NUMBER

5e. TASK NUMBER

5f. WORK UNIT NUMBER

7. PERFORMING ORGANIZATION NAME(S) AND ADDRESS(ES)
University of Texas Southwestern Medical Center
Dallas, TX 75390
AND ADDRESS(ES)

8. PERFORMING ORGANIZATION REPORT NUMBER

9. SPONSORING / MONITORING AGENCY NAME(S) AND ADDRESS(ES)
U.S. Army Medical Research and Materiel Command
Fort Detrick, Maryland 21702-5012

10. SPONSOR/MONITOR'S ACRONYM(S)

11. SPONSOR/MONITOR'S REPORT NUMBER(S)

12. DISTRIBUTION / AVAILABILITY STATEMENT
Approved for Public Release; Distribution Unlimited

13. SUPPLEMENTARY NOTES

14. ABSTRACT
Prostate cancer (PCa) is the second highest cancer mortality among male cancer in USA. This disease is still incurable because PCa once becomes metastatic and develops drug resistance when cancer cells undergo epithelial-to-mesenchymal transition (EMT) and acquire cancer stem cell (CSC) phenotypes. Emerging evidence has shown that the presence of metastatic PCa is associated with CSC phenotype that is likely associated with its resistance to radiation or chemotherapy. The preliminary data from this study clearly demonstrate that several tumor suppressor microRNAs (miRNAs) involved in regulating these processes are often degraded by IFIT5. Also, elevated IFIT5 is associated with PCa malignancy. Thus, this study will delineate the mechanism of IFIT5 in tumor suppressor miRNA degradation, and examine IFIT5 gene regulation. By determining its clinical correlation, this study will provide valuable biomarker(s) for lethality of PCa, which will an immediate impact on patient prognosis and selection for more suitable agent.The outcome of this study will provide a better understanding of miRNAs biogenesis associated with aggressive PCa exhibiting CSC phenotypes. Most importantly, the long-term the impact of this study will generate more effective therapeutic strategy of CRPC.

15. SUBJECT TERMS
None listed

16. SECURITY CLASSIFICATION OF:			17. LIMITATION OF ABSTRACT	18. NUMBER OF PAGES	19a. NAME OF RESPONSIBLE PERSON
a. REPORT	b. ABSTRACT	c. THIS PAGE			USAMRMC
Unclassified	Unclassified	Unclassified	Unclassified	73	19b. TELEPHONE NUMBER *(include area code)*

Table of Contents

Page

1. INTRODUCTION

MicroRNAs (miRNAs) are small non-coding RNA molecules that regulate gene expression by post-transcriptional degradation or translational repressions by recognizing the 3'-UTR sequence of target mRNA from the specific seed sequence (ca. 2-7 nucleotides) of miRNAs (1). miRNAs have been shown to regulate approximate 60% protein-coding genes via post-transcriptional suppression by facilitating mRNA degradation, or translational inhibition. In general, miRNAs are initially transcribed into a long primary transcript by RNA polymerase II similar to cellular mRNA, and sequentially processed by Drosha and Dicer-mediated endonuclease cleavage to become mature miRNA (2-4). Nevertheless, miRNA biogenesis becomes more complicated when miRNAs are derived from the same gene cluster controlled by the same promoter and yet some is processed with different efficiency at the precursor or mature level (5, 6), which adds more complexities into the scheme of gene regulation.

Epithelial-to-mesenchymal transition (EMT) is considered an initial step for cancer cells to acquire the metastatic potentials. In PCa, many studies have demonstrated the relationship of the onset of EMT phenotypes with cancer metastasis. Knowing EMT as a normal physiologic process takes place during embryonic development, therefore, the cancer cells undergoing EMT appear to have higher potential to acquire cancer stem cell (CSC) phenotypes (7). However, the molecular mechanism(s) associated with EMT or CSC in PCa is not fully understood.

Our preliminary data clearly indicated that elevated IFIT5 is associated with malignant PCa and IFIT5 can target many miRNAs with tumor suppressive function in preventing EMT and CSC, in which IFIT5 can be as a potential therapeutic target. Therefore, it is critical to dissect the mechanism of IFIT5 in degrading miRNA or the regulation of IFIT5. Also, significant clinical correlation of elevated IFIT5 expression in PCa specimens prompt us to explore IFIT5 as prognostic marker for PCa.

REFERENCES

1. Aalto AP, Pasquinelli AE. (2012) Small non-coding RNAs mount a silent revolution in gene expression. Curr Opin Cell Biol., 24:333-340.
2. Bartel DP. (2004) MicroRNAs: genomics, biogenesis, mechanism, and function. Cell, 116:281-297.
3. Feng Y, *et al*. (2011) Drosha processing controls the specificity and efficiency of global microRNA expression. Biochimica et Biophysica Acta, 1809:700-707.
4. Winter J, *et al*. (2009) Many roads to maturity: microRNA biogenesis pathways and their regulation. Nat. Cell Biol. 11:228-234.
5. Chaulk SG, *et al.* (2011) Role of pri-miRNA tertiary structure in miR-17~92 miRNA biogenesis. RNA Biol., 8:1105-1114.
6. Chakraborty S, *et al.* (2012) Pri-miR-17-92a transcript folds into a tertiary structure and autoregulates its processing. RNA, 18:1014-1028.
7. Garg M. (2015) Targeting microRNAs in epithelial-to-mesenchymal transition-induced cancer stem cells: therapeutic approaches in cancer. Expert Opin. Ther. Targets., 19:285-297.

2. KEYWORDS

Epithelial-to-mesenchymal transition, cancer stem cell, IFIT5, XRN1 microRNA, microRNA turn over.

3. ACCOMPLISHMENTS

Major goals and accomplishments

Aim 1 Dissect the mechanism of IFIT5-mediated miRNA turnover.

Major Task: Unveil new machinery of miRNA turnover**.**

Preliminary data from the proposal indicate that the presence of IFIT5 can specifically decrease mature miR-363 from miR-106a-363 cluster in PCa cells. In addition, the data show this suppression is caused by the degradation of precursor-miR-363. Although IFIT5 is known to bind to 5'-end of tRNA, its role and action in miRNA turnover remains undetermined. To dissect the mechanism of action of IFIT5, we performed immuneprecipitation and mass spectroscopy and identified XRN1, an exoribonuclease, as a potential interactive partner. In order to show the requirement of both IFIT5 and XRN1 for miR-363 degradation, we generated recombinant IFIT5 then combined with XRN1 enzyme and pre-miR-363 transcript to perform in vitro miRNA degradation assay, the result (Fig. 1A) showed both proteins are required for miR-363 degradation. Furthermore, we generated 2 mutant pre-miR-363 constructs: one with 5'-end six nucleotides single stranded overhang (SS^6Mut pre-miR-363) and the other with double-stranded blunt end (DSMut pre-miR-363) (Fig. 2B) to show that DSMut pre-miR-363 is more resistant to the degradation of IFIT5-XRN1 complex. Similarly, DSMut pre-miR-363 vector can produce more miR-363 compared with SS^6Mut pre-miR-363 vector transfected into PCa cells (Fig. 1C). Functionally, DSMut pre-miR-363 vector exhibits higher inhibitory effect of cell invasion compared with wild type pre-miR-363 or SS^6Mut pre-miR-363 vector (Fig. 1D). Overall, IFIT5-XRN1 complex represents a unique machinery of miRNA turnover.

Milestone: Manuscript on mechanism of miRNA turnover**.**

A manuscript is currently reviewed by Nature Communication.

Aim 2 Determine the regulation of IFIT5 gene in PCa progression.

Major Task: Identify key regulator(s) and inducer(s) of IFIT5 gene expression**.**

IFIT family is first characterized as an interferon (IFN)-induced gene. We therefore examine the effect of all the IFNs on IFIT5 expression and the results indicate that all the IFNs can induce IFIT5 protein as well as mRNA expression (Fig. 2A). Among three IFNs, IFNγ elevation is associated in PCa patients after radiation and hormonal therapy. We decided to focus the action of IFNγ and further identified that the induction of IFIT5 mRNA by IFNγ was the result of transcriptional activation mediated by STAT1 signaling using IFIT5 gene promoter construct (Fig. 2B). Consistently, IFNγ was able to induce the expression of IFIT5 protein and mRNA in a dose-dependent manner (Fig. 2C). In addition, DAB2IP is able to inhibit IFIT5

expression (Fig. 2D), we believe that DAB2IP can intervene IFNγ-induced IFIT5 through STAT1 pathway.

Aim 3 Evaluate IFIT5 as a prognostic marker in PCa patients.

Major Task: Determine IFIT5 as a potential prognostic marker for PCa

Currently, we are collecting clinical specimens in order to have enough samples for analyses. Nevertheless, we have performed some preliminary test by treating fresh specimens with IFNγ for IFIT5 induction in an *ex vivo* culture system. As shown in Fig. 3, fresh human PCa specimens treated with IFNγ at different concentrations were determined the expression of IFIT5, ZEB1, Slug that exhibited a dose-dependent elevation. These data suggest that IFNγ could induce EMT in PCa cells via IFIT5 pathway.

What opportunities for training and professional development have the project provided?
This project provides excellent training opportunities for molecular cell biology, tumor biology and pathohistologic techniques.

How were the results disseminated to communities of interest?
Currently, we have submitted two manuscripts under review and one abstract in the annual AUA meeting.

What do you plan to do during the next reporting period to accomplish the goals?
Currently, our progress is right on the target based on original SOW; we have completed Specific Aim1 and submitted one manuscript. For the next reporting period, we expect to delineate (1) the regulation of IFIT5 and its role in cancer stem cell development (2) the correlation of IFIT5 with clinical manifestation of human PCa.

4. IMPACT

What was the impact on the development of the principal discipline(s) of the project? What was the impact on other disciplines?
Emerging evidence has shown that the presence of metastatic CRPC is associated with cancer stem cell phenotype that is likely associated with its resistance to radiation or chemotherapy. This study clearly demonstrates that several tumor suppressor microRNAs (miRNAs) involved in regulating these processes are often degraded by IFIT5. Also, elevated IFIT5 is associated with PCa malignancy. Thus, this study will delineate the mechanism of IFIT5 in tumor suppressor miRNA degradation, and examine IFIT5 gene regulation. By determining its clinical correlation, this study will provide valuable biomarker(s) for lethality of PCa, which will an immediate impact on patient prognosis and selection for more suitable agent.
In addition, we have discovered a new function of IFIT5 complex as many tumor suppressor miRNA degradation machinery in PCa. This discovery can certainly be applied onto other cancer types such as renal and liver cancers. In addition, the knowledge derived from this study can be used for designing better miRNA for therapeutic purpose.

What was the impact on technology transfer?
Nothing to Report.

What was the impact on society beyond science and technology?
Nothing to report.

5. CHANGES/PROBLEMS

Nothing to report.

6. PRODUCTS

Lo, U., Pong, R.C., Yang, D., Gandee, L., Hernandez, E., Santoyo, J., Ma, S-H., Huang, J., Tseng, S-F., Raj, G., He, D., Lai, C.H., Lin, H., Hsieh, J.T. (2017) Interferon induces epithelial-to-mesenchymal transition (EMT) in prostate cancer by eliciting a new mechanism of action on the turnover of tumor suppressor microRNAs. Nat. Comm. (revised).

Lo, U., Lee, C.F., Lee, M-S., Hsieh, J.T. (2017) The role and mechanism of epithelial-to-mesenchymal transition in prostate cancer progression. Int. J. Mol. Sci. (submitted).

7. PARTICIPANTS AND OTHER COLLABORATING ORGANIZATIONS

Name: U-Ging Lo
Project Role: Research Scientist
Researcher Identifier (e.g. ORCID ID): none
Nearest person month worked: 12
Project: Perform all the experiments.
Funding Support: DOD

Name: Payal Kapur
Project Role: collaborator
Researcher Identifier (e.g. ORCID ID): none
Nearest person month worked: 0.3
Project: Pathologic examination of specimens.
Funding Support: DOD, NIH

Has there been a change in the active other support of the PD/PI(s) or senior/key personnel since the last reporting period?
Nothing to Report.

What other organizations were involved as partners?
Nothing to Report.

8. SPECIAL REPORTING REQUIREMENTS

None.

9. Appendices

Figure 1. Characterization of precursor miR-363 degradation and its effect on cell invasion. (**A**) In vitro miRNA degradation of native pre-miR-363 after incubating with recombinant IFIT5 protein (rIFIT5), XRN1 enzyme (XRN1) or combination of XRN1 and rIFIT5 at 37°C for 45, 90 and 120 min. (**B**) In vitro miRNA degradation of SS6Mut- or DSMut-pre-miR-363 after incubating with rIFIT5, XRN1 or combination of XRN1 and rIFIT5 at 37°C for 0, 30, 45, 60, 90, and 120 min. (**C**) Induction of mature miR-363 in cells transfected with SS6Mut pre-miR-363 or DSMut pre-miR-363 plasmids and IFIT5 siRNA after normalizing with the control vector (Vec). (Con=control siRNA). (**D**) The effect of Native, DSMut-or SS6Mut-pre-miR-363 on cell invasion in PC3 cells. Cells invaded at the lower bottom at the Transwell were stained with crystal violet and counted. Each bar represents mean ± SD of nine fields of counted cell numbers. (* $p<0.05$).

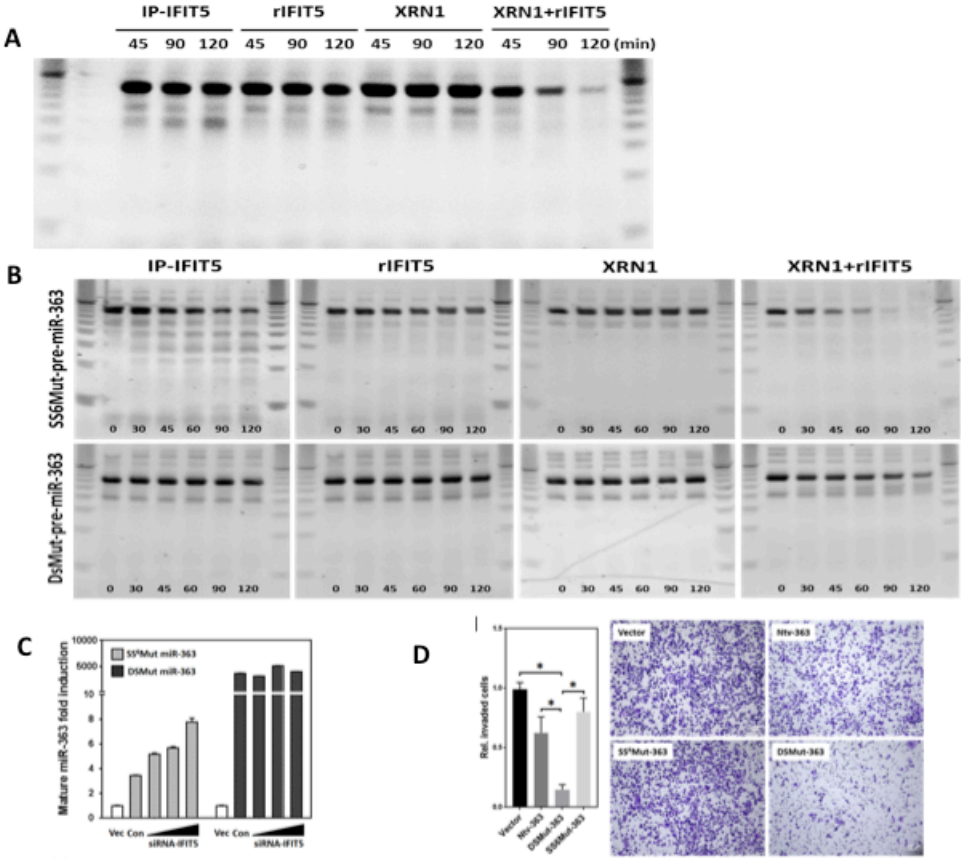

Figure 2. **The regulation of IFIT5 gene expression in PCa cells** (**A**) Left and middle panel: Induction of IFIT5 by protein and mRNA level by IFNα, IFNβ and IFNγ treatment for 48hrs in PC3 cells. Right panel: Expression level of miR-363 in PC3 cells treated with IFNα, IFNβ and IFNγ for 48 hrs. (**B**) IFNγ-induced IFIT5 promoter activity in PC3 cells with shRNA knockdown of STAT1 (shSTAT1), compared to control shRNA (shCon). (**C**) Dose dependent induction of IFIT5 protein and mRNA level in LAPC4-KD and PC3 cells treated with IFNγ (10 and 20 ng/ml) for 48 hrs. (**D**) The inhibitory effect of DAB2IP on IFIT5 protein expression in PC3 cells.

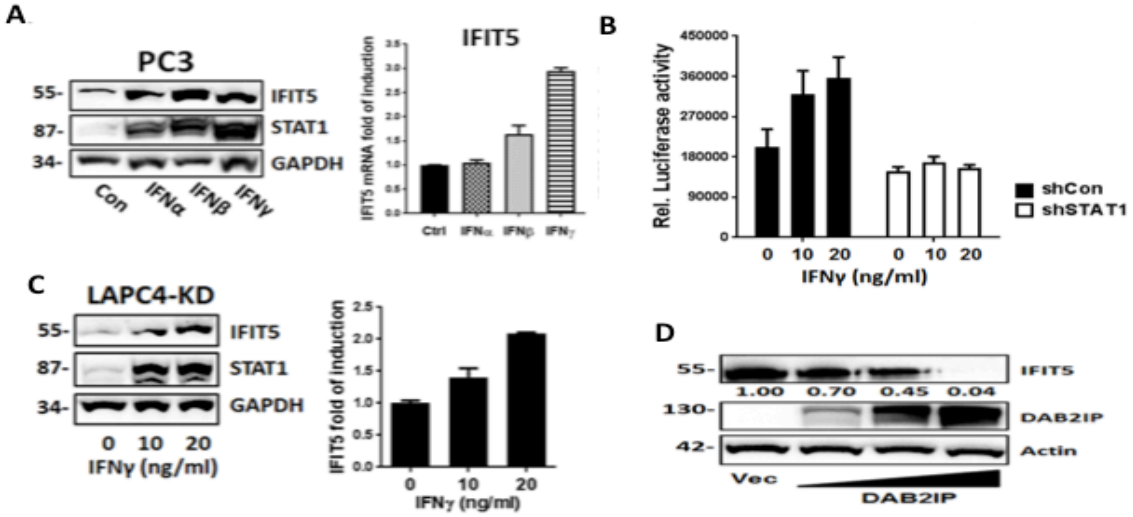

Figure 3. Induction level of IFIT5, ZEB1, and Slug mRNA expression in ex vivo culture of human PCa specimens. Tumor specimens were treated with IFNγ (0, 25 and 100 ng/ml) for 48 hrs and total cellular RNAs were extracted and subjected to real time-RTPCR. The relative mRNA expression was normalized with control from individual specimen.

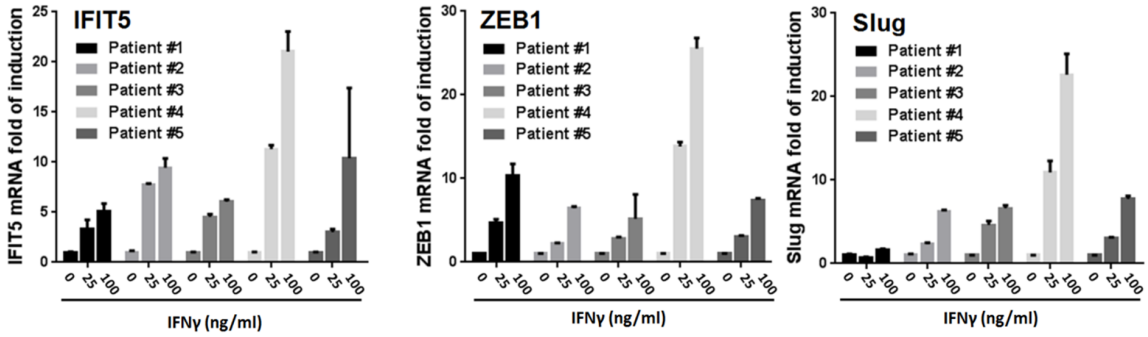

Interferon-γ induces epithelial-to-mesenchymal transition in cancer by eliciting a new mechanism of tumor suppressor microRNAs processing

U-Ging Lo[1], Rey-Chen Pong[1], Diane Yang[1], Leah Gandee[1], Elizabeth Hernandez[1], Andrew Dang[1], Chung-Jung Lin[1], John Santoyo[1], Shi-Hong Ma[1], Jun Huang[2], Shu-Fen Tseng[3], Loredana Moro[4], Arnaldo A. Arbini[5], Payal Kapur[6], Ganesh Raj[1], Dalin He[2], Chih-ho Lai[7], Ho Lin[8], and Jer-Tsong Hsieh[1,9]

[1]Department of Urology, University of Texas Southwestern Medical Center, Dallas, TX 75390, USA; [2]Department of Urology, The First Affiliated Hospital, Medical School of Xi'an Jiaotong University, Xi'an 710049, China; [3]Department of Bioengineering, University of Texas at Arlington, Arlington, TX 76019, USA; [5]Institute of Biomembranes, Bioenergetics and Molecular Biotechnologies, National Research Council, Bari, Italy; [6]Department of Pathology, NYU Langone Medical Center, New York, NY, 10016; [6]Department of Pathology, University of Texas Southwestern Medical Center, Dallas, TX 75390, USA; [7]Department of Microbiology and Immunology, Graduate Institute of Biomedical Sciences, College of Medicine, Chang Gung University, Taoyuan 33302, Taiwan; [8]Department of Life Sciences, National Chung Hsing University, Taichung 40402, Taiwan; [9]Graduate Institute of Cancer Biology, China Medical University Hospital, Taichung 40447, Taiwan, Republic of China

Running Title: IFN-elicited EMT via microRNA turnover

Key Words: IFIT5, XRN1, microRNA-363, EMT

Footnotes

Jer-Tsong Hsieh, Ph.D., jt.hsieh@utsouthwestern.edu, Phone: 214-648-3988; Fax: 214-648-8786; 5323 Harry Hines Blvd., J8-134 Dallas, TX 75390, USA.

ABSTRACT

Interferon-γ (IFNγ) is a potent cytokine implicated in anti-tumor immunity. We demonstrate that IFNγ has pro-tumor effect by inducing epithelial-to-mesenchymal transition (EMT) from different cancer cell models. IFNγ activates JAK-STAT signaling pathway leading to the transcription of IFN-stimulated genes (ISGs), such as interferon-induced tetratricopeptide repeat 5 (IFIT5). We unveil a new function of IFIT5 complex as turnover machinery for microRNAs (miRNA), which specifically degrades pre-miR-363 from the miR-106a-363 cluster, as well as mediates the turnover ofpre-miR-101 and pre-miR-128 that share similar 5'-end structure with pre-miR-363. Noticeably, these suppressive miRNAs have similar function by targeting EMT transcription factors in prostate, renal and liver cancer cells. Clinically, IFIT5 is highly elevated in high-grade prostate cancer and its expression inversely correlates with these suppressive miRNAs. Altogether, this study unveils pro-tumorigenic role of the IFN pathway via a new mechanism of action, which certainly raises concern about its clinical application.

Interferon-γ (IFNγ) is first characterized as a cytokine associated with antivirus as well as antitumor activities during cell-mediated innate immune response[1,2]. Mechanistically, IFNs can activate JAK-STAT signaling pathway after binding to type II receptors and induce the transcriptional activation of a variety of IFN-stimulated genes (ISGs) resulting in diverse biologic responses[3]. Among ISGs, interferon-induced tetratricopeptide repeat (IFIT) family members are highly inducible. They are viral RNA binding proteins[4] and a part of antiviral defense mechanisms. They disrupt viral replication and/or viral RNA translation in host cells. Among IFIT orthologs, human IFIT1, IFIT2 and IFIT3 form a complex through the tetratricopeptide repeats (TPR) to degrade viral RNA. However, the functional role of IFIT5 is not fully understood since it acts solely as a monomer that can not only bind directly to viral RNA molecules via its convoluted RNA-binding cleft, but also endogenous cellular RNAs with a 5'-end phosphate cap, including transfer RNAs (tRNA) [5,6]. In this study, we demonstrate a new function of IFIT5 in regulating microRNAs (miRNA) turnover.

miRNAs are a large family of short sequence single-stranded noncoding RNAs, which have been shown to regulate approximately 60% of protein-coding genes via post-transcriptional suppression, mRNA degradation, or translation inhibition[7,8]. Many miRNAs are associated with different stages of tumor development. These miRNAs are divided into onco-miRNAs and tumor suppressor miRNAs based on the function of their target genes. Similar to most protein-coding genes, miRNA genes can be regulated at transcriptional or post-transcriptional level [9]. Unlike most eukaryotic protein genes, several miRNAs such as miR-106a-363[10] and miR-17-92 are clustered together to generate a polycistronic primary transcript [11-13], which further complicates the regulatory scheme of miRNA biogenesis. For example, miR-363 belongs to the polycistronic miR-106a-363 cluster containing six miRNAs (miR-106a, miR-18b, miR-20b, miR-19b-2, miR-92a-2 and miR-363). Unlike the other five miRNAs with similar seed sequences and functions as the oncogenic miR-17-92 cluster [14], miR-363 acts as a tumor suppressor that is able to inhibit the transcriptional factor responsible for epithelial-to-mesenchymal transition (EMT). We further delineate that the differential regulation of miR-363 from this miR-106a-363 cluster is mediated by unique miRNA turnover machinery composed of IFIT5 and XRN1, which appears to be a novel, and previously unreported function of IFIT5.

Based on the discovery of IFIT5-mediated miRNA turnover machinery, additional miRNAs such as miR-101 and miR-128 were also identified as IFIT5-targeted miRNAs and these miRNAs are able to target different EMT transcriptional factors such as ZEB1 and Slug. Clinically, loss of these miRNAs is associated with tumor grade of prostate cancer, which is inversely correlated with elevated IFIT5 mRNA level. On the other hand, IFIT5 mRNA expression is correlated with ZEB1 and Slug mRNA expression in prostate cancer specimens. Functionally, IFIT5 plays a key role in IFNγ –induced EMT. Taken together, we conclude that IFN is a promoting factor in prostate cancer progression.

RESULTS

The specific correlation between DAB2IP and miR-363 expression Disabled homolog 2-interacting protein (DAB2IP) is known as a potent regulator in EMT leading to cancer metastasis [15,16]. However, the detailed mechanism of action of DAB2IP is not fully characterized. As emerging evidence demonstrates the critical role of miRNA in the EMT process of prostate cancer (PCa), we therefore performed miRNA microarray screening (Fig. S1A and B) that resulted in the identification of a unique miRNA, miR-363 that is significantly decreased in DAB2IP-knockdown (KD) cells. The down-regulation of miR-363 in DAB2IP-KD cells was further validated in not only prostate cell lines (LAPC-4, RWPE1, PC3 and PNT1A) (Fig. 1A) but also renal cell lines such as 786O-KD and HK2-KD (Fig. S1C). Ectopic expression of DAB2IP in C4-2Neo or LAPC4-KD cells (Fig. 1B), or HEK293 (Fig. S1D) was able to induce mature miR-363 levels in a dose-dependent manner, indicating that DAB2IP could modulate miR-363 expression.

miR-363 is located in the polycistronic miR-106a-363 cluster that is first transcribed into a single primary miRNA containing the entire sequence of the cluster genes. We therefore examined the effect of DAB2IP on the expression levels of primary transcript of miR-106a-363. In contrast to the significant down-regulation of mature miR-363 in DAB2IP-KD cells, the expression levels of primary miR-106a-363 were similar between DAB2IP-positive and -negative cells (Fig. 1C). Also, the expression levels of pre-miR-363 showed no significant difference between these cells (Fig. 1D). Noticeably, only the mature miR-363 levels dramatically decreased in DAB2IP-KD cells (i.e., LAPC4-KD and RWPE1-KD) (Fig. 1E). On the other hand, only the mature miR-363 levels increased significantly in C4-2 (Fig. 1E)

and HEK293 cells (Fig. S1E) with ectopic expression of DAB2IP. These findings indicate that DAB2IP specifically regulates miR-363 maturation process.

The effect of IFIT5 on the distinct biogenesis of miR-363 from the miR-106a-363 cluster In order to elucidate the machinery responsible for miR-363 maturation process, the protein candidates were immunoprecipitated using synthetic pre-miR-363 RNA molecule as bait and analyzed by LC-MS/MS (Table S1). This experiment unveiled IFIT5 protein as a potential hit. The steady-state levels of IFIT5 mRNA and protein were inversely correlated with DAB2IP (Fig. S2A). IFIT5 is characterized as a viral RNA or cellular tRNA binding protein and has, so far, not been known to bind to microRNAs. Therefore, the specific RNA-protein association between pre-miR-363 and IFIT5 was further validated using RNA pull-down and western blot analysis between DAB2IP-negative and –positive PCa cell lines (Fig. 2A). This inhibitory effect of DAB2IP on IFIT5 expression was further confirmed by the ectopic expression of DAB2IP in LAPC4-KD (Fig. 2B), C4-2Neo (Fig. 2C), LNCaP (Fig. S2B), and HEK293 cells (Fig. S2C).

To further examine whether IFIT5 plays a critical role in DAB2IP-mediated miR-363 maturation, we ectopically expressed IFIT5 in DAB2IP-positive cells. This resulted in a significant reduction of mature miR-363 levels but not the other mature miRNAs from the same cluster (Fig. 2D). In addition, on applying different IFIT5 small interfering RNA (siRNA) on LAPC4-KD cells, the levels of mature miR-363 correlated with the reduction in the endogenous IFIT5 mRNA levels (Fig. S2D). Thus, the IFIT5-C siRNA was chosen for further analysis. Reduced IFIT5 resulted in a significant elevation of mature miR-363 in a dose-dependent manner (Fig. S2E). Despite the significantly elevated mature miR-363 in IFIT5-KD cells, the levels of mature miR-106a, miR-18b, miR-20b, miR-19b-2 and miR-92a-2 remained relatively unchanged (Fig. 2E and S2F). Also, the expression levels of pre-miR-363 and other pre-miRNAs from the same cluster remained unchanged in these IFIT5-KD cells (Fig. S2G). Taken together, the data suggest that IFIT5 can specifically inhibit miR-363 maturation from the miR-106a-363 cluster.

The effect of IFNs on the biogenesis of miR-363 from the miR-106a-363 cluster Since the IFIT protein family is a typical ISG, we further confirmed that IFIT5 was induced by all the IFNs (Fig. 2F). Meanwhile, a significant reduction of miR-363 was also observed under the

same condition (Fig. 2F). Among three IFNs, IFNγ appears to have the most potent effect in suppressing miR-363. We therefore, used IFNγ to examine its impact on IFIT5 downstream target miRNAs. We first identified that the induction of IFIT5 mRNA by IFNγ was the result of transcriptional activation mediated by STAT1 signaling using IFIT5 gene promoter construct (Fig. 2G). Moreover, IFNγ was able to induce the expression of IFIT5 protein and mRNA in a dose-dependent manner (Fig. 2H and I) and significantly reduce mature miR-363 levels compared to other miRNAs in miR-106a-363 cluster (Fig 2H and I, S2H and I). These data support a key mediator role of IFIT5 in IFNγ-mediated miR-363 suppression.

The functional role of miR-363 in EMT DAB2IP is known to inhibit EMT[16]. Based on the predicted sequences and gene profiling modulated by miR-363 in DAB2IP-KD cells, Slug/SNAI2 mRNA appears to be a potential candidate target gene. We therefore transfected miR-363 expression into KD cells, we observed huge expression levels (ranging 10,000 folds) then selected stable clone with low expression (<100 folds) to avoid any potential artifact. Indeed, suppression of Slug/SNAI2 mRNA levels was detected in miR-363 expressing cells compared to controls (Fig. 3A and B, and S3A). By constructing both wild type Slug/SNAI2 3'UTR (Slug-WT3'UTR) and mutant Slug/SNAI2 3'UTR (Slug-Mut^{363}3'UTR) reporter genes, a significant reduction of the Slug-WT3'UTR but not the Slug-Mut^{363}3'UTR activity was detected in RWPE-1-KD cells (Fig. 3C) and LAPC4-KD cells (Fig. S3B).

Slug/SNAI2 is known to promote EMT by suppressing the expression of epithelial markers such as E-Cadherin. As expected, an elevation of E-cadherin mRNA and protein was observed in miR-363 overexpressing RWPE-1-KD cells (Fig. 3D and E) and LAPC4-KD cells (Fig. S3C). In contrast, the expression of both mRNA and protein levels of Vimentin, a mesenchymal marker, were suppressed in both cell lines compared to controls (Fig. 3D and S3C). Functionally, miR-363 significantly reduced cell migration in miR-363 expressing RWPE-1-KD (Fig. 3F) and LAPC4-KD cells (Fig. S3D). In contrast, inhibition of miR-363 in both RWPE-1 and C4-2D2 cell lines results in diminished cell migration motility (Fig. 3G). We also noticed that cells collected from the lower chamber of a Transwell exhibited lower miR-363 levels than the upper chamber (Fig. S3D). Moreover, we restored Slug/SNAI2 level in miR-363-expressing cells that, in turn, resulted in a dose-dependent reduction of E-Cadherin mRNA and protein levels, as well as an elevation in Vimentin mRNA and protein

levels in RWPE-1-KD cells (Fig. 3H) and LAPC4-KD cells (Fig. S3E), further validating Slug/SNAI2 as the key target gene of miR-363-mediated EMT inhibition.

We further observed an inverse relationship between miR-363 and IFIT5 expression in renal (such as 293T and 786O) and liver (such as HepG2) cancer cell lines in addition to prostate cancer cells (Fig. S4A). Knocking down of IFIT5 in these cell lines resulted in a significant elevation of mature miR-363 level (Fig. S4B). Similar inhibitory effect on EMT was observed in these cells: HepG2 (Fig. S4C, D and E), 293T (Fig. S4F, G and H), and 786O cell lines (Fig. S4I, J and K), by the ectopic expression of miR-363. These data indicate that miR-363 can suppress EMT by targeting the expression of Slug and Vimentin.

The mechanism of IFIT5 on miR-363 turnover at precursor level In a recent study, IFIT5 has been suggested to suppress virus replication by targeting the 5'-phosphate end of single stranded viral RNAs for rapid turnover[6]. Thus, we examined whether IFIT5 has a direct impact on the stability of pre-miR-363. In fact, pre-miR-363 RNA prepared from *in vitro* transcription was relatively stable at 37°C (Fig. S5A). However, the presence of IFIT5 protein complex significantly increased the turnover rate of pre-miR-363 RNA (Fig. S5A), indicating that the degradation of pre-miR-363 is accelerated by the IFIT5 protein complex. To examine the specificity of IFIT5 in the acceleration of pre-miR-363 degradation, we determined the *in vitro* degradation rate of pre-miR-92a-2 (immediate adjacent to miR-363) in the presence of IFIT5 and found no significant change (Fig. 4A). Previous studies [4,5] indicate that IFIT5 protein binds to viral RNA molecules at either 5'-phosphate cap or 5'-tri-phosphate group. By comparing the 5'-end structure between pre-miR-92a-2 and pre-miR-363, we hypothesized that a single nucleotide (uracil) overhang in pre-miR-363, in contrast to the double-stranded blunt end in pre-miR-92a-2 is critical for IFIT5 recognition. Therefore, we generated 2 mutant pre-miR-363 constructs: one with 5'-end six nucleotides single stranded overhang (SS^6Mut pre-miR-363) and the other with double-stranded blunt end (DSMut pre-miR-363) (Fig. 4B) to test their stabilities. The result (Fig. 4C) indicated that the expression levels of primary miR-363 from either native or mutants were similar. However, the expression levels of pre-miR363 or mature miR-363 derived from SS^6Mut were significantly lower than those from native or DSMut form (Fig. 4C), indicating that the 5'-end structure of pre-miR-363 dictates the stability of miR-363 maturation. Similar pattern of mature miR-363

expression was also detected in RWPE1-KD and LAPC4-KD cells (Fig. S5B and C). Upon determining the *in vitro* degradation rates of pre-miR-363, SS^6Mut and DSMut pre-miR-363 RNA molecules, as we expected, SS^6Mut pre-miR-363 was very sensitive to IFIT5 whereas DSMut pre-miR-363 was the most resistant one (Fig. 4D). Furthermore, we observed a steady elevation of SS^6Mut -derived mature miR-363 level in a dose-dependent manner in the presence of an incremental IFIT5 siRNA, while the expression of DSMut-derived mature miR-363 remained at high levels and was not affected by IFIT5 siRNA (Fig. 4E). Meanwhile, using RNA pull-down assay, SS^6Mut pre-miR-363 exhibited higher affinity to IFIT5 protein than DSMut pre-miR-363 (Fig. 4F). In contrast, DICER, one of the key endoribonuclease for miRNA maturation, exhibited higher interaction with DSMut pre-miR-363 than SS^6Mut pre-miR-363. It appeared that DSMut pre-miR-363 was more stable than SS^6Mut pre-miR-363 *in vivo* (Fig. S5C). Thus, DSMut exhibited a significant effect on inhibiting EMT (Fig. S5D) evidenced by elevated E-cadherin expression (Fig. 4G), which resulted in diminishing cell migration of LAPC4-KD cells (Fig. S5E) and inhibiting cell invasion of PC3 cells (Fig. 4H). These data conclude that IFIT5 recognizes the unique 5'-end overhanging structure of pre-miR-363 to elicit its degradation.

To further demonstrate the specificity of this unique 5'-end structure of pre-miRNA, we also generated a mutant construct of pre-miR-92a-2 with single nucleotide at 5'-overhang (SS^1Mut pre-miR-92a-2) (Fig. S5F) which is similar to the 5'-end of pre-miR-363 (Fig. 4B). Using RNA pull-down assay, we observed an increased interaction between SS^1Mut pre-miR-92a-2 and IFIT5 protein, compared to native pre-miR-92a-2 (Fig. S5F). Moreover, the degradation rate of SS^1Mut pre-miR-92a-2 increased in the presence of IFIT5 complex, compared to that of pre-miR-92a-2 (Fig. S5G). Thus, we believe that IFIT5-mediated precursor miRNAs turnover is determined by the 5'-end overhanging structure.

The role of XRN1 in IFIT5-mediated miR-363 turnover Although IFIT5 can elicit miR-363 turnover, IFIT5 doesn't possess ribonuclease activity. To determine if a ribonuclease is associated with the IFIT5-pre-miR-363 complex, we further examined LC-MS/MS results and identified an exoribonuclease candidate-XRN1. XRN1 is known to regulate mRNA stability via cleavage of de-capped 5'-monophosphorylated mRNA [17,18] and a recent study also implied its potential role in miRNA turnover [19]. Indeed, an interaction was observed between IFIT5

and XRN1 protein in LAPC4-Con cells transfected with Flag-tagged IFIT5 (Fig. 5A). Using three different XRN1 siRNAs in LAPC4-KD cells, we showed that the elevated expression levels of miR-363 correlated with the diminished level of XRN1 protein (Fig. 5B and S6A). Similar to IFIT5-KD, data from XRN1-KD cells clearly demonstrated that only mature miR-363 exhibited a significant accumulation whereas the levels of other mature miRNAs (miR-106a, miR-18b, miR-20b, miR-19b-2, and miR-92a-2) remained relatively unchanged (Fig. 5C).

Also, by incubating immunoprecipitated XRN1 proteins (Fig. S6B) with native, SS^6Mut or DSMut pre-miR-363 RNA molecules, a significant increase of both native and SS^6Mut pre-miR-363 degradation was detected in a time-dependent manner, whereas DSMut pre-miR-363 levels remained unchanged (Fig. 5D and S6B), implying that the IFIT5 binding structure in the 5'-end of pre-miR-363 is critical for recruiting XRN1. Indeed, upon ectopic transfection of IFIT5 cDNA into XRN1-expressing LAPC4-Con cells, the presences of IFIT5 significantly facilitated the degradation rate of SS^6Mut -pre-miR-363 (Fig. 5E and S6C). On the other hand, loss of XRN1 in IFIT5-expressing LAPC4-Con cells diminished the degradation rate of SS^6Mut pre-miR-363 (Fig. 5F and S6D). These findings provide further evidence for the specific function of IFIT5-XRN1 complex in miR-363 turnover. In addition, using recombinant IFIT5 protein with or without XRN1 enzyme, the result (Fig. 5G and S6E) clearly indicated that both IFIT5 and XRN1 proteins are required to degrade pre-miR-363 transcript in vitro. Also, the SS^6Mut pre-miR-363 is more sensitive to IFIT5-XRN1 complex than DSMut pre-miR-363 (Fig. 5H and S6F). Overall, these data demonstrate that the IFIT5-XRN1 complex is responsible for the processing of pre-miR-363.

The effect of IFNγ on miR-101, miR-128, and miR-363 processing mediated by IFIT5 To survey additional miRNAs subjected to IFIT5-mediated precursor miRNA degradation, we performed miRNA microarray using IFIT5-expressing LAPC4-Con and IFIT5-depleted LAPC4-KD cells and unveiled miR-101 and miR-128 as candidates. We further confirmed that the presence of IFIT5 reduced the expression of mature miR-101 and miR-128 as well as miR-363 in PC3 cell line (Fig. 6A). In contrast, IFIT5 KD in LAPC4-KD cells increased the expression of all three miRNAs (Fig S7A). Also, XRN1 KD in IFIT5-expressing cells could rescue the expression levels of mature miR-363, miR-101 and miR-128 (Fig. S7B), indicating

the requirement of XRN1 in IFIT5 complex in degrading these miRNAs. Similarly, IFNγ treatment resulted in reducing the expression of miR-101, miR-128 and miR-363 (Fig. 6B). This inhibitory effect can be reversed or diminished by knocking down IFIT5, STAT1 or XRN1 (Fig. 6C). Similarly, overexpression of DAB2IP in PC3 cells also diminished the inhibitory effect of IFNγ on the suppression of miR-101, miR-128 and miR-363 level (Fig. S7C), supporting the key role of IFIT5 in IFNγ-elicited precursor miRNAs processing.

By comparing the precursor structures of miR-101 and miR-128, it appeared that both pre-miR-101 and pre-miR-128 have similar 5'-end structure with pre-miR-363, we therefore generated 2 mutant constructs: one with 5'-end single stranded overhang (SSMut) and the other with double-stranded blunt end (DSMut) (Fig. 6D and G) to test their expression in IFIT5-expressing PC3 and LAPC4-KD cell lines. As we expected, DSMuts were resistant to IFIT5-elicited miRNA degradation and resulted in elevated expression of mature miRNA in PC3 (Fig. 6E and H) and LAPC4-KD cells (Fig. S7E and F). Based on the 3'UTR sequence, ZEB1 mRNA was predicted as a target for both miR-101 and miR-128 (Fig. S7D), and the results indeed indicated that both miR-101 and miR-128 could suppress ZEB1 mRNA levels (Fig. S7D). Again, DSMuts appeared to degrade ZEB1 mRNA and protein more efficiently in PC3 (Fig. 6E and H) and LAPC4-KD cells (Fig. S7E and F), which are correlated with the suppression of cell invasion in PC3 cells (Fig. 6F and I) and cell migration in LAPC4-KD cells (Fig. S7E and F). In addition, we also examined the effect of IFIT5 or IFNγ on the expression level of miR-200 family members involved in the suppression of Slug and ZEB1. The result (Fig. S7G) indicated that the impact of IFNγ or IFIT5 on EMT was not mediated through miR-200 members. Overall, the effect of IFIT5-XRN1 complex on pre-miR-101/128/363 processing is unique with respect to the similar 5'-end overhang structure.

The effect of IFNγ on EMT mediated by IFIT5 Based on the mechanism of action of IFIT5-XRN1 complex in the degradation of miRNAs that can target EMT factors, we further examined whether IFNγ could elicit EMT by suppressing these miRNAs via STAT1 signal axis and its downstream effector-IFIT5/XRN1complex. Indeed, IFNγ treatment increased the PC3 cell migration (Fig. 7A) and invasion (Fig. 7B) that was diminished in the absence of IFIT5 (Fig. 7A, 7B and S8A) or STAT1 (Fig.7B, S7A and B), which is consistent with the expression of EMT factors (Slug and ZEB1) or decrease in the mesenchymal marker

(Vimentin) or increase in the epithelial marker (E-cadherin) (Fig. 7C and D). As we expected the expression of all these three miRNAs was inhibited by IFNγ in a dose-dependent manner (Fig. 6C) and IFNγ failed to suppress the expression of these miRNAs in the absence of XRN1, STAT1 or IFIT5 (Fig. 6C) in which no induction of Slug and ZEB1 mRNA was detected (Fig. 7E). Similarly, the effect of IFNγ on Slug and ZEB1 mRNA induction was diminished in cells with overexpression of miR-101, miR-128 or miR-363 (Fig. S8C).

Apparently, IFNγ is capable of inducing EMT at low concentrations that are not anti-tumorigenic (Fig. S8D); its direct anti-tumor activity is known at much higher concentration (>1000 ng/ml)[20]. These data provide new evidence that IFNγ is a potent inducer of EMT via STAT1-IFIT5/XRN1 signal axis of miRNA regulation.

The clinical correlation of IFIT5, miRNAs and EMT biomarkers in PCa To examine the in vivo effect of IFNγ on PCa metastasis and the role of IFIT5 in this event, we treated control (shCon) and IFIT5-KD cells with IFNγ for 48hrs then cells were injected intravenously into SCID animal via tail vein. IFNγ treatment significantly increases the number and size of metastatic nodules at lung parenchyma, in contrast, the loss of IFIT5 dramatically reduces metastasis of PCa with or without IFNγ (Fig. 8A, 8B and Table S2). Furthermore, we demonstrated the effect of IFNγ on EMT clinically, we employed an *ex vivo* culture system[21] . Human PCa specimens and data indicated that IFNγ was able to induce the expression of IFIT5, ZEB1, Slug (Fig. 8D) and Vimentin (Fig. S9A) gene whereas miR-101 and miR-363 levels were significantly inhibited (Fig. S9B). We also surveyed the expression status of IFIT5 from different grades of PCa specimens and data (Fig. 8E) indicate that IFIT5 mRNA levels were significantly elevated in the high-grade PCa. As expected, the expression pattern of miR-363, miR-101 and miR-128 levels was opposite to that of IFIT5 (Fig. 8E), which is consistent with our observation from tissue culture cell lines. In contrast, miR-92a-2 and miR-19b-2 immediately adjacent to miR-363 known as oncomirs exhibited an elevated expression pattern in PCa tissues compared to normal tissues (Fig. S9C), supporting the specificity of IFIT5 on miRNA degradation. Meanwhile, data from PCa specimens also demonstrated a similar correlation between IFIT5 mRNA and these 3 miRNAs (Fig. 8F). In addition, analyses of expression of EMT factors or markers demonstrated a positive correlation between IFIT5 and ZEB1 (or Slug) (Fig. 8G), and Vimentin (Fig. S9D). Similar correlation between IFIT5 and

ZEB1 (or Slug) was also observed in TCGA dataset of renal cell carcinoma (Fig. S9E) and hepatocellular carcinoma (Fig. S9F).

DISCUSSION

Immunologic features of the tumor microenvironment play a critical role in tumor immunity. PCa lesion is often found to have many different kinds of infiltrated immune cells such as macrophages, dendritic cells and tumor-infiltrating lymphocytes[22,23]. Instead of eliciting tumor immunity, these immune cells with secreting cytokines are capable of facilitating PCa development. For example, a study has demonstrated that fibroblast growth factor 11 (FGF11) released by the recruited CD4+ T cells can induce cell invasion by increasing matrix metalloproteinase 9 (MMP9) in PCa cells[24]. In addition, IL-4 produced from CD4+ T cells has shown to increase PCa cell survival and proliferation by activating the JNK signaling pathway in cancer cells[25]. Moreover, IL-17 secreted from T helper cells is capable of facilitating PCa invasiveness by increasing several EMT transcription factors and MMP7[26]. On the other hand, IFNγ, a type II interferon derived predominantly from CD4+/CD8+ lymphocytes and NK cell, is shown to have antitumor activities during innate immune response. Also, IFNγ has been used as a therapeutic agent exhibiting anti-proliferative[27], anti-metastatic[28], pro-apoptotic[29-32] and anti-angiogenesis[33-36] effects in various cancer types. However, several reports indicate that IFNγ could also facilitate tumor progression. For example, IFNγ can elicit CD4+ T-cell loss and impair secondary anti-tumor immune responses after initial immunotherapy using tumor-bearing mouse model [37]. In colorectal carcinoma, IFNγ has been shown to facilitate the induction of indoleamine 2, 3 dioxygenase (IDO) that induces the production of kynurenines metabolites and impairs the function of surrounding T cells[38]. In addition to its role in immune modulation, blockade of IFNγ receptor (IFNGR) can inhibit peritoneal disseminated tumor growth of ovarian cancer[39]. Noticeably, serum IFNγ levels become elevated after radiotherapy in PCa patients[40]. Nevertheless the effect of IFNγ on the overall survival of PCa patients remains controversial[41]. In our study, we provide additional evidence that IFNγ and two other subtypes (Fig. 2F) are able to induce EMT, leading to cancer invasiveness via IFIT5-mediated turnover of tumor suppressor miRNAs (Fig. 8F). We also noticed that low concentration of IFNγ capable of inducing EMT

exhibited no cytotoxicity (Fig. S7). To strengthen the evidence of IFN-induced EMT clinically, we treated ex vivo PCa explants with IFN and data indicated that IFN could induce similar elevations of IFIT5 and EMT transcriptional factors and suppression of miR-101 and -363 (Fig. 8). Taken together, these data show that IFNγ has a biphasic effect on tumor development. Nevertheless, the pro-tumorigenic effect of IFNγ at low concentration is expected to raise a concern for its application as an anti-tumor or immunotherapeutic agent.

Unlike other IFIT family proteins, IFIT5 is characterized as a monomeric protein that is capable of binding to viral RNA with 5'-triphosphate group[4] as well as a broad spectrum of cellular RNA with either 5'-monophosphate or 5'-triphosphate group, including tRNA and other RNA polymerase III transcripts[6]. However, the interaction of IFIT5 with miRNA is largely unknown. Knowing that precursor miRNA shares a similar stem loop structure with tRNA and a precursor miRNA still retains 5'-monophosphate group after processing from its primary transcript, we are able to show that IFIT5 is capable of interacting with 5'-end of pre-miRNA molecules. After binding to pre-miRNA, IFIT5 recruits XRN1 to form unique miRNA turnover complex (Fig. 5). For the first time, we demonstrated that the specificity of miRNA recognition by IFIT5 is mainly determined by the 5'-end overhang structure of pre-miRNAs (Figs. 4, 6). Interestingly, these 3 tumor suppressor miRNAs (i.e., miR-101, miR-128 and miR-363) share similar 5'-end structure in their pre-miRNA and function in suppressing EMT despite of targeting different EMT transcriptional factors such as ZEB1 and Slug. To conclude, our study provides a new functional role of IFIT5 in miRNA biogenesis (Fig. 8F), particularly, a new understanding of differential regulation of cluster miRNAs.

Until now, the clinical correlation of IFIT5 in PCa is largely undetermined. In this study, we were able to demonstrate that the expression of IFIT5 is elevated in high-grade tumor and inverse correlation between IFIT5 and miR-101, -128 and -363 in PCa tumor specimens as well as from PCa TCGA database; this correlative relationship was not observed in other members of the miR-106a-363 cluster. In addition, a significant clinical correlation between IFIT5 and EMT transcription factors (ZEB1 or Slug) was observed from PCa TCGA dataset, which further validate the regulatory network of IFIT5-miRNAs-EMT. Taken together, data from clinical specimens provide a strong supportive evidence for a key role of IFIT5 in EMT

in human PCa and its underlying mechanism of turnover of tumor suppressor miRNAs. Also, the knowledge gained from this study can be applied on the design of miRNA therapy.

It appears that this novel mechanism of IFIT5 is not only limited to PCa cells but also in renal cancer and liver cancer cells. Thus, more studies are expected for determining the pro-tumorigenic effect of IFNγ in other cancers. Nevertheless, data from the clinical correlation of IFIT5 in PCa suggest that IFIT5 can be a potential target for PCa therapy.

MATERIALS AND METHODS

Cell lines, Clinical specimens, and Plasmid constructs

Stable DAB2IP-KD and control (Con) prostatic cell lines were generated from RWPE-1, PC-3 and LAPC4 cell lines using shRNA[16]. Stable IFIT5 KD (shIFIT5) and control (shCon) prostatic cell lines were generated from LAPC4-KD, RWPE1-KD and C4-2Neo cell lines using pLKO-shIFIT5 from Academia Sinica, Taipei, Taiwan. Stable IFIT5-overexpressing (IFIT5) and control (Vec) prostatic cell lines were generated from LAPC4-Con, RWPE1-Con and C4-2D2 cell lines using pcDNA3.1-3XFlag-IFIT5 plasmid from Dr. Collins. LAPC4 derived from PCa patients with lymph node metastasis was maintained in Iscove Dulbecco's Modified Eagle's Medium (DMEM) (Invitrogen) containing 10% fetal bovine serum (FBS). RWPE-1 derived from normal prostate epithelial cells immortalized with human papillomavirus 18 was maintained in Keratinocyte medium (Invitrogen) containing 10% FBS. The androgen-sensitive LNCaP cell line derived from PCa patients with lymph node metastasis was maintained in RPMI-1640 medium (Invitrogen) containing 10% FBS. C4-2 and PC-3, androgen-independent lines, were maintained in RPMI-1640 medium containing 10% FBS. Renal cancer 786O cell lines were maintained in RPMI-1640 medium (Invitrogen) containing 10% FBS, whereas hepatocellular carcinoma HepG2 and 293T cell lines are maintained in DMEM (Invitrogen) containing 10% FBS.

A total of 41 PCa specimens obtained from UT Southwestern Tissue Bank. All the specimens were collected from 6-mm core punch from radical prostectomy and examined by pathologist to determine tumor grade then subjected to RNA extraction. The Institutional Review Board of UT Southwestern approved the tissue procurement protocol for this study, and appropriate informed consent was obtained from all patients.

All the plasmid constructs are described in Supplemental information.

Cell transfection

Cells ($2.5x10^5$) were seeded in 60-mm dish at 60-70% confluence before transfection. According to manufacturer's protocol, transfection of plasmids was using either Xfect Reagent (Clontech) or EZ Plex transfection reagent (EZPLEX), and transfection of siRNA was using Lipofectamine® RNAiMAX reagent (Life Technology). Transient transfection was carried out 48 hrs post-transfection to harvest cell for further analyses. In addition, the stable clones (CL) were established after 2 weeks in the antibiotic selective medium.

RNA isolation and quantitative real-time RT-PCR (qRT-PCR)

Small and large RNA were isolated and purified using mirVana miRNA Isolation Kit (Life Technologies). Small RNA (250 ng) was subjected to miScript II RT kit (QIAGEN) then 2.5 µl cDNA was applied to a 25-µL reaction volume using miScript SYBR Green PCR kit (QIAGEN) in iCycler thermal cycler (Bio-Rad). All primer sequences are listed in Table S3. The relative expression levels of precursor and matured miRNAs from each sample were determined by normalizing to SNORD95 small RNA. Large RNA (2 µg) was subjected to SuperScript VILO cDNA synthesis kit (Invitrogen) then 2.5 µl cDNA was applied to 25-µl reaction volume using SYBR Green ER qPCR SuperMix (Invitrogen). The relative expression levels of DAB2IP, IFIT5, E-cadherin, and Vimentin, ZEB1 and Slug/SNAI2 mRNA from each sample were determined by normalizing to 18S mRNA.

Western blot analysis

Cells were washed with PBS and lysed in lysis buffer [50mMTris-HCl (pH 7.5), 150 mM NaCl, 0.1% Triton X-100, 1 mM sodium orthovanadate, 1 mM sodium fluoride, 1 mM sodium pyrophosphate, 10 mg/mL, aprotinin, 10 mg/mL leupeptin, 2 mM phenylmethylsulfonyl fluoride, and 1 mM EDTA] for 60 mins on ice. Cell lysates were spin down at 20,000 xg for 20 mins at 4°C. Protein extracts were subjected to SDS-PAGE using Bolt 4-12% Bis-Tris Plus gel (Invitrogen), and transferred to nitrocellulose membrane using Trans-Blot Turbo Transfer system (BIORAD). Membranes were incubated with primary antibodies against DAB2IP, E-Cadherin, Vimentin, ZEB1, Slug/SNAI2, XRN1, IFIT5 and

Flag at 4 °C for 16-18 hrs, and horseradish peroxidase-conjugated secondary antibodies at room temperature for 1.5 hrs. Results were visualized with ECL chemiluminescent detection system (Pierce ThermoScientific). The relative protein expression level in each sample was normalized to actin or GAPDH.

Immunoprecipitation (IP) assay

Cells were harvested and protein lysates were prepared freshly before performing IP assay. Flag antibody (Sigma) or XRN1 antibody (AbCam) was incubated with 50 µl of Dynabeads® protein G (Novex, Life Technology) at room temperature for 15 mins. Subsequently, total 300 µg of protein lysate was incubated with the Dynabead-conjugated antibody at 4°C for 16-18 hrs. After washing, the elutes were subjected to SDS-PAGE using Bolt 4-12% Bis-Tris Plus gel (Invitrogen), and transferred to a nitrocellulose membrane using Trans-Blot Turbo Transfer system (BIORAD). Membranes were then subjected to western blot probed with different antibodies.

Luciferase reporter assay

Cells ($8X10^4$) were seeded onto 12-well plates at 75% confluence before transfection. pCMV-miR-363 plasmid was co-transfected with psiCHECK2-Slug3'UTR-WT or psiCHECK2-Slug3'UTR-Mut^{363} plasmid into LAPC4-KD and RWPE-1-KD cells using Xfect Reagent (Clontech). Cells were harvested and lysed with Passive Lysis buffer (Promega) at 48 hrs after transfection. Luciferase activity was measured using the Dual-luciferase reporter assay (Promega) on the Veritas Microplate Luminometer (Turner Biosystems). Results were expressed as the relative light unit by normalizing the firefly luciferase activity with Renilla luciferase activity. Each experiment was performed in triplicates.

***In vitro* transcription of precursor miRNA**

The PCR-amplified DNA fragment of T7-promoter-precursor-miRNAs was separated by 2% agarose gel electrophoresis and purified using Mermaid SPIN kit (MP Biomedicals), then subjected to *in vitro* transcription assay using T7 High Yield RNA synthesis kit (New England Biolabs). DNA template (750 ng) was mixed with T7 High Yield 10X buffer, NTP mixture (ATP, GTP, CTP and UTP), and T7 RNA polymerase then incubated at 37°C for 16 hrs. The

precursor miRNA molecules was first treated with DNase I for 15 mins at 25°C and purified by acid phenol-chloroform extraction and ethanol precipitation. The molecular size and sequence of each purified precursor miRNA was confirmed by gel electrophoresis and qRT-PCR respectively.

RNA pull-down assay

The *in vitro* transcribed precursor miRNA was subjected to RNA pull down assay using Pierce Magnetic RNA-Protein Pull-Down Kit (ThermoScientific). An approximate 100 pmol of precursor miRNA were incubated with 10X RNA Ligase reaction buffer, RNase inhibitor, Biotinylated Cytidine Bisphosphate, and T4 RNA ligase at 16°C for 16 hrs. The biotinylated precursor miRNA was then purified and incubated with streptavidin magnetic beads for 30 mins at room temperature. Whole cell lysates were freshly prepared immediately before RNA pull-down assay and 200 μg of protein extract was mixed with the biotinylated precursor miRNA conjugated to streptavidin magnetic beads and incubated at 4°C for 1 hr. The magnetic beads were washed 4 times before elution. Proteins associated with precursor miRNA were eluted and subjected to SDS-PAGE using Bolt 4-12% Bis-Tris Plus gel. Gel bands were stained with Coomassie blue and subjected to LC-MS/MS analysis.

***In vitro* pre-miRNA degradation assay**

The *in vitro* transcribed precursor miRNAs were incubated with immunoprecipitated IFIT5 or XRN1 in the elution buffer at 37°C on a thermomixer (Eppendorf), then the RNA-containing buffer were collected at indicated time points and subjected to 15% TBE-Urea gel electrophoresis. To quantify the degradation of precursor miRNA, the 15% TBE-Urea gel was then stained with GelRed^{TM} Nucleic Acid Gel Stains (VWR) and visualized under UV light in the AlphaImager devise (Protein Simple). The RNA bands were quantified by Multiplex band analysis (AlphaView Software) and the rate of degradation was calculated from each time point normalized to time zero.

***In vitro* migration and invasion assay**

Cells ($1X10^5$ or $4X10^4$) in the serum-free medium were plated on the upper chamber (8-μm pore size) of Transwell (Corning) with or without Matrigel coating for invasion or migration

assay, respectively, while lower chamber contained medium supplemented with 10% FBS. After 5 days, cells that had transmigrated to the lower chamber were fixed by 4% paraformaldehyde, stained and visualized under microscope. Quantification of migratory cells was carried out with crystal violet staining and measurement at OD_{555nm}. Each experiment was performed in triplicates.

***Ex vivo* culture of patient-derived PCa explants**

Following informed consent, fresh PCa tissues were obtained from men undergoing radical prostatectomy at the hospitals of the University of Texas Southwestern Medical Center (Dallas, TX). The ex vivo culture was performed as previously described[21]. Briefly, fresh PCa tissue was dissected into 1 mm^3 cube and placed on a Gelatin sponge (Novartis, East Hanover, NJ) bathed in RPMI-1640 media supplemented with 10% heat-inactivated FBS, 100 units/mL penicillin-streptomycin, 0.01 mg/mL hydrocortisone and 0.01 mg/mL insulin (Sigma). In addition, to the media, was added either vehicle, IFNγ (25 ng/ml) or IFNγ (100 ng/ml). Tissues were cultured at 37 °C for 48 hrs then paraffin-embedded for pathologic examination of Gleason's grade or frozen in liquid nitrogen for RNA purification.

Statistics analysis

Statistics analyses were performed by using GraphPad Prism software. Statistical significance was evaluated using Student t-test. $P<0.05$ was considered a significant difference between compared groups and marked with an asterisk. The statistical association between miR-363 and IFIT5 expression among different grades of human PCa was evaluated with regression correlation analysis.

ACKNOWLEDGMENTS

We thank Dr. Collins (University of California, Berkeley) for providing IFIT5 cDNA constructs, Dr. Dong (Emory University, Atlanta) for providing the psiCHECK2-Slug3'UTR plasmid. Drs. Kou-Juey Wu (China Medical University, Taichung, Taiwan) and Dr. Vimal Selvaraj (Cornell University, Ithaca) for the helpful discussion. This work was supported by grants from the United States Army (W81XWH-11-1-0491 and W81XWH-16-1-0474 to JTH) and (W81XWH-14-1-0249 to UGL), and the Ministry of Science and Technology in Taiwan (MOST103-2911-I-005-507 to HL)

References

1 Hildenbrand, B. *et al.* Immunotherapy of patients with hormone-refractory prostate carcinoma pre-treated with interferon-gamma and vaccinated with autologous PSA-peptide loaded dendritic cells--a pilot study. *The Prostate* **67**, 500-508, doi:10.1002/pros.20539 (2007).

2 Street, S. E., Cretney, E. & Smyth, M. J. Perforin and interferon-gamma activities independently control tumor initiation, growth, and metastasis. *Blood* **97**, 192-197 (2001).

3 de Veer, M. J. *et al.* Functional classification of interferon-stimulated genes identified using microarrays. *J Leukoc Biol* **69**, 912-920 (2001).

4 Abbas, Y. M., Pichlmair, A., Gorna, M. W., Superti-Furga, G. & Nagar, B. Structural basis for viral 5'-PPP-RNA recognition by human IFIT proteins. *Nature* **494**, 60-64, doi:10.1038/nature11783 (2013).

5 Katibah, G. E. *et al.* tRNA binding, structure, and localization of the human interferon-induced protein IFIT5. *Molecular cell* **49**, 743-750, doi:10.1016/j.molcel.2012.12.015 (2013).

6 Katibah, G. E. *et al.* Broad and adaptable RNA structure recognition by the human interferon-induced tetratricopeptide repeat protein IFIT5. *Proceedings of the National Academy of Sciences of the United States of America* **111**, 12025-12030, doi:10.1073/pnas.1412842111 (2014).

7 Aalto, A. P. & Pasquinelli, A. E. Small non-coding RNAs mount a silent revolution in gene expression. *Current opinion in cell biology* **24**, 333-340, doi:10.1016/j.ceb.2012.03.006 (2012).

8 Schickel, R., Boyerinas, B., Park, S. M. & Peter, M. E. MicroRNAs: key players in the immune system, differentiation, tumorigenesis and cell death. *Oncogene* **27**, 5959-5974, doi:10.1038/onc.2008.274 (2008).

9 Obernosterer, G., Leuschner, P. J., Alenius, M. & Martinez, J. Post-transcriptional regulation of microRNA expression. *Rna* **12**, 1161-1167, doi:10.1261/rna.2322506 (2006).

10 Dylla, L. & Jedlicka, P. Growth-promoting role of the miR-106a~363 cluster in Ewing sarcoma. *PloS one* **8**, e63032, doi:10.1371/journal.pone.0063032 (2013).

11 Chow, T. F. *et al.* The miR-17-92 cluster is over expressed in and has an oncogenic effect on renal cell carcinoma. *The Journal of urology* **183**, 743-751, doi:10.1016/j.juro.2009.09.086 (2010).

12 Diosdado, B. *et al.* MiR-17-92 cluster is associated with 13q gain and c-myc expression during colorectal adenoma to adenocarcinoma progression. *British journal of cancer* **101**, 707-714, doi:10.1038/sj.bjc.6605037 (2009).

13 Wong, P. *et al.* The miR-17-92 microRNA polycistron regulates MLL leukemia stem cell potential by modulating p21 expression. *Cancer research* **70**, 3833-3842, doi:10.1158/0008-5472.CAN-09-3268 (2010).

14 Landais, S., Landry, S., Legault, P. & Rassart, E. Oncogenic potential of the miR-106-363 cluster and its implication in human T-cell leukemia. *Cancer research* **67**, 5699-5707, doi:10.1158/0008-5472.CAN-06-4478 (2007).

15 Min, J. *et al.* An oncogene-tumor suppressor cascade drives metastatic prostate cancer by coordinately activating Ras and nuclear factor-kappaB. *Nature medicine* **16**, 286-294, doi:10.1038/nm.2100 (2010).
16 Xie, D. *et al.* Role of DAB2IP in modulating epithelial-to-mesenchymal transition and prostate cancer metastasis. *Proceedings of the National Academy of Sciences of the United States of America* **107**, 2485-2490, doi:10.1073/pnas.0908133107 (2010).
17 Jones, C. I., Zabolotskaya, M. V. & Newbury, S. F. The 5' --> 3' exoribonuclease XRN1/Pacman and its functions in cellular processes and development. *Wiley interdisciplinary reviews. RNA* **3**, 455-468, doi:10.1002/wrna.1109 (2012).
18 Nagarajan, V. K., Jones, C. I., Newbury, S. F. & Green, P. J. XRN 5'-->3' exoribonucleases: structure, mechanisms and functions. *Biochimica et biophysica acta* **1829**, 590-603, doi:10.1016/j.bbagrm.2013.03.005 (2013).
19 Jones, C. I. *et al.* The 5'-3' exoribonuclease Pacman (Xrn1) regulates expression of the heat shock protein Hsp67Bc and the microRNA miR-277-3p in Drosophila wing imaginal discs. *RNA biology* **10**, 1345-1355, doi:10.4161/rna.25354 (2013).
20 Wall, L., Burke, F., Barton, C., Smyth, J. & Balkwill, F. IFN-gamma induces apoptosis in ovarian cancer cells in vivo and in vitro. *Clinical cancer research : an official journal of the American Association for Cancer Research* **9**, 2487-2496 (2003).
21 Ravindranathan, P. *et al.* Peptidomimetic targeting of critical androgen receptor-coregulator interactions in prostate cancer. *Nature communications* **4**, 1923, doi:10.1038/ncomms2912 (2013).
22 Gannon, P. O. *et al.* Characterization of the intra-prostatic immune cell infiltration in androgen-deprived prostate cancer patients. *Journal of immunological methods* **348**, 9-17, doi:10.1016/j.jim.2009.06.004 (2009).
23 Strasner, A. & Karin, M. Immune Infiltration and Prostate Cancer. *Frontiers in oncology* **5**, 128, doi:10.3389/fonc.2015.00128 (2015).
24 Hu, S. *et al.* Infiltrating T cells promote prostate cancer metastasis via modulation of FGF11-->miRNA-541-->androgen receptor (AR)-->MMP9 signaling. *Molecular oncology* **9**, 44-57, doi:10.1016/j.molonc.2014.07.013 (2015).
25 Roca, H. *et al.* IL-4 induces proliferation in prostate cancer PC3 cells under nutrient-depletion stress through the activation of the JNK-pathway and survivin up-regulation. *Journal of cellular biochemistry* **113**, 1569-1580, doi:10.1002/jcb.24025 (2012).
26 Zhang, Q. *et al.* Interleukin-17 promotes prostate cancer via MMP7-induced epithelial-to-mesenchymal transition. *Oncogene*, doi:10.1038/onc.2016.240 (2016).
27 Aune, T. M. & Pogue, S. L. Inhibition of tumor cell growth by interferon-gamma is mediated by two distinct mechanisms dependent upon oxygen tension: induction of tryptophan degradation and depletion of intracellular nicotinamide adenine dinucleotide. *J Clin Invest* **84**, 863-875 (1989).
28 Addison, C. L. *et al.* The CXC chemokine, monokine induced by interferon-gamma, inhibits non-small cell lung carcinoma tumor growth and metastasis. *Human gene therapy* **11**, 247-261, doi:10.1089/10430340050015996 (2000).
29 Fukui, T. *et al.* Significance of apoptosis induced by tumor necrosis factor-alpha and/or interferon-gamma against human gastric cancer cell lines and the role of the p53 gene. *Surg Today* **33**, 847-853 (2003).

30 Burke, F., East, N., Upton, C., Patel, K. & Balkwill, F. R. Interferon gamma induces cell cycle arrest and apoptosis in a model of ovarian cancer: enhancement of effect by batimastat. *Eur J Cancer* **33**, 1114-1121 (1997).

31 Suk, K. *et al.* Interferon gamma (IFNgamma) and tumor necrosis factor alpha synergism in ME-180 cervical cancer cell apoptosis and necrosis. IFNgamma inhibits cytoprotective NF-kappa B through STAT1/IRF-1 pathways. *The Journal of biological chemistry* **276**, 13153-13159 (2001).

32 Chung, T. W. *et al.* Induction of indoleamine 2,3-dioxygenase (IDO) enzymatic activity contributes to interferon-gamma induced apoptosis and death receptor 5 expression in human non-small cell lung cancer cells. *Asian Pac J Cancer Prev* **15**, 7995-8001 (2014).

33 Strieter, R. M., Kunkel, S. L., Arenberg, D. A., Burdick, M. D. & Polverini, P. J. Interferon gamma-inducible protein 10 (IP-10), a member of the C-X-C chemokine family, is an inhibitor of angiogenesis. *Biochemical and biophysical research communications* **210**, 51-57, doi:10.1006/bbrc.1995.1626 (1995).

34 Saiki, I. *et al.* Inhibition of tumor-induced angiogenesis by the administration of recombinant interferon-gamma followed by a synthetic lipid-A subunit analogue (GLA-60). *International journal of cancer* **51**, 641-645 (1992).

35 Sun, T. *et al.* Inhibition of tumor angiogenesis by interferon-gamma by suppression of tumor-associated macrophage differentiation. *Oncology research* **21**, 227-235, doi:10.3727/096504014X13890370410285 (2014).

36 Ribatti, D. *et al.* Angiogenesis in a human neuroblastoma xenograft model: mechanisms and inhibition by tumour-derived interferon-gamma. *British journal of cancer* **94**, 1845-1852, doi:10.1038/sj.bjc.6603186 (2006).

37 Berner, V. *et al.* IFN-gamma mediates CD4+ T-cell loss and impairs secondary antitumor responses after successful initial immunotherapy. *Nature medicine* **13**, 354-360, doi:10.1038/nm1554 (2007).

38 Mellor, A. L. & Munn, D. H. Tryptophan catabolism prevents maternal T cells from activating lethal anti-fetal immune responses. *Journal of reproductive immunology* **52**, 5-13 (2001).

39 Abiko, K. *et al.* IFN-gamma from lymphocytes induces PD-L1 expression and promotes progression of ovarian cancer. *British journal of cancer* **112**, 1501-1509, doi:10.1038/bjc.2015.101 (2015).

40 Tanji, N. *et al.* Circulating Cytokine Levels in Patients with Prostate Cancer: Effects of Neoadjuvant Hormonal Therapy and External-beam Radiotherapy. *Anticancer research* **35**, 3379-3383 (2015).

41 Hastie, C. Interferon gamma, a possible therapeutic approach for late-stage prostate cancer? *Anticancer research* **28**, 2843-2849 (2008).

671 **Figures and figure legends**

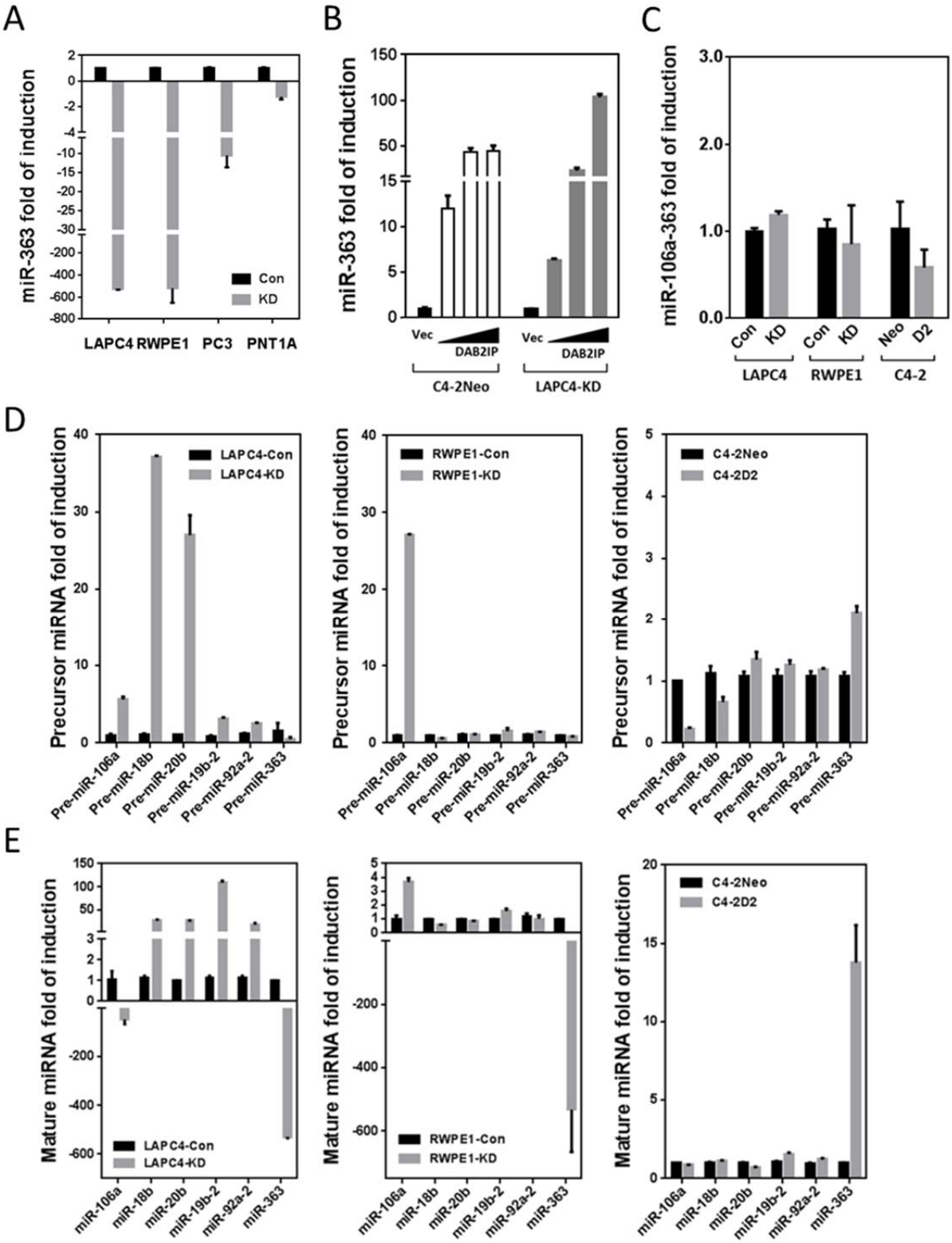

672

673

674 **Figure 1. The effect DAB2IP on miR-363 expression in prostate cell lines.**

675 (A) Expression levels of miR-363 in DAB2IP-knockdown (KD) prostate cell lines after
676 normalizing with the control (Con). (B) Induction of miR-363 by ectopic expression of
677 DAB2IP in C4-2Neo and LAPC4-KD cell lines after normalizing with the control vector
678 (Vec). (C) Expression levels of primary miR-106a-363 in DAB2IP-positive and-negative
679 sublines. (D) Expression levels of precursor miRNAs (miR-106a, miR-18b, miR-20b, miR-
680 19b-2, miR-92a-2 and miR-363) in DAB2IP-positive and-negative cells. (E) Expression
681 levels of mature miRNAs (miR-106a, miR-18b, miR-20b, miR-19b-2, miR-92a-2 and miR-
682 363) in DAB2IP-positive and-negative cells.

683

684

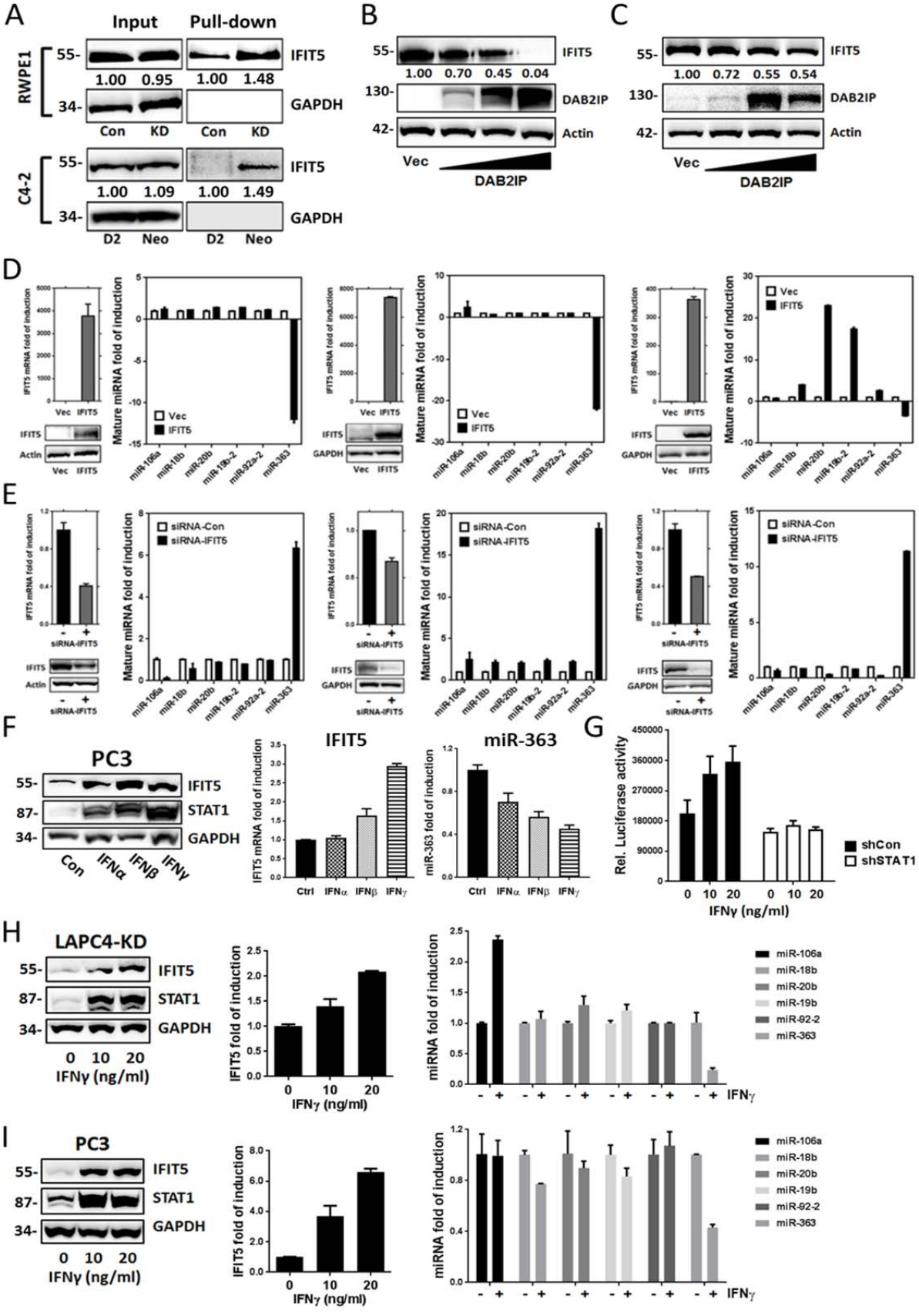
A
Input
Pull-down
RWPE1
55-
IFIT5
1.00 0.95 1.00 1.48
34-
GAPDH
Con KD Con KD
C4-2
55-
IFIT5
1.00 1.09 1.00 1.49
34-
GAPDH
D2 Neo D2 Neo
B
55-
IFIT5
1.00 0.70 0.45 0.04
130-
DAB2IP
42-
Actin
Vec
DAB2IP
C
55-
IFIT5
1.00 0.72 0.55 0.54
130-
DAB2IP
42-
Actin
Vec
DAB2IP
D
IFIT5 mRNA fold of induction
Vec IFIT5
IFIT5
Actin
GAPDH
Mature miRNA fold of induction
Vec
IFIT5
miR-106a
miR-18b
miR-20b
miR-19b-2
miR-92a-2
miR-363
E
IFIT5 mRNA fold of induction
siRNA-IFIT5
siRNA-Con
Mature miRNA fold of induction
F
PC3
55-
IFIT5
87-
STAT1
34-
GAPDH
Con
IFNα
IFNβ
IFNγ
IFIT5
IFIT5 mRNA fold of induction
Ctrl IFNα IFNβ IFNγ
miR-363
miR-363 fold of induction
G
Rel. Luciferase activity
shCon
shSTAT1
0 10 20 0 10 20
IFNγ (ng/ml)
H
LAPC4-KD
55-
IFIT5
87-
STAT1
34-
GAPDH
0 10 20
IFNγ (ng/ml)
IFIT5 fold of induction
0 10 20
IFNγ (ng/ml)
miRNA fold of induction
miR-106a
miR-18b
miR-20b
miR-19b
miR-92-2
miR-363
- + - + - + - + - + - + IFNγ
I
PC3
55-
IFIT5
87-
STAT1
34-
GAPDH
0 10 20
IFNγ (ng/ml)
IFIT5 fold of induction
0 10 20
IFNγ (ng/ml)
miRNA fold of induction
miR-106a
miR-18b
miR-20b
miR-19b
miR-92-2
miR-363
- + - + - + - + - + - + IFNγ

685

Figure 2. The impact of IFIT5 on miR-363 maturation from the miR-106a-363 cluster.

(A) The interaction between IFIT5 protein and pre-miR-363 in DAB2IP-positive and –negative cells using RNA pull down assay. (B-C) Suppression of IFIT5 protein expression by ectopic transfecting DAB2IP into LAPC4-KD (B) and C4-2Neo (C) cells after normalizing with the control vector (Vec). (D) Expression levels of mature miRNAs (miR-106a, miR-18b, miR-20b, miR-19b-2, miR-92a-2 and miR-363) in IFIT5-expressing (IFIT5) LAPC4-Con, C4-2D2 and RWPE1-Con cells after normalizing with the control vector (Vec). (E) Expression levels of mature miRNAs (miR-106a, miR-18b, miR-20b, miR-19b-2, miR-92a-2 and miR-363) in IFIT5-siRNA knockdown (+) LAPC4-KD (left panel), C4-2Neo (middle panel) and RWPE1-KD (right panel) cells compared to the control siRNA (-). (F) Left and middle panel: Induction of IFIT5 by protein and mRNA level by IFNα, IFNβ and IFNγ treatment for 48hrs in PC3 cells. Right panel: Expression level of miR-363 in PC3 cells treated with IFNα, IFNβ and IFNγ for 48hrs. (G) IFNγ-induced IFIT5 promoter activity in PC3 cells with shRNA knockdown of STAT1 (shSTAT1), compared to control shRNA (shCon). (H-I) Left and middle panel: Dose dependent induction of IFIT5 protein and mRNA level in LAPC4-KD and PC3 cells treated with IFNγ (10 and 20ng/ml) for 48 hrs. Right panel: Expression levels of mature miRNAs (miR-106a, miR-18b, miR-20b, miR-19b-2, miR-92a-2 and miR-363) in LAPC4-KD and PC3 cells treated with IFNγ (10 and 20 ng/ml) for 48 hrs.

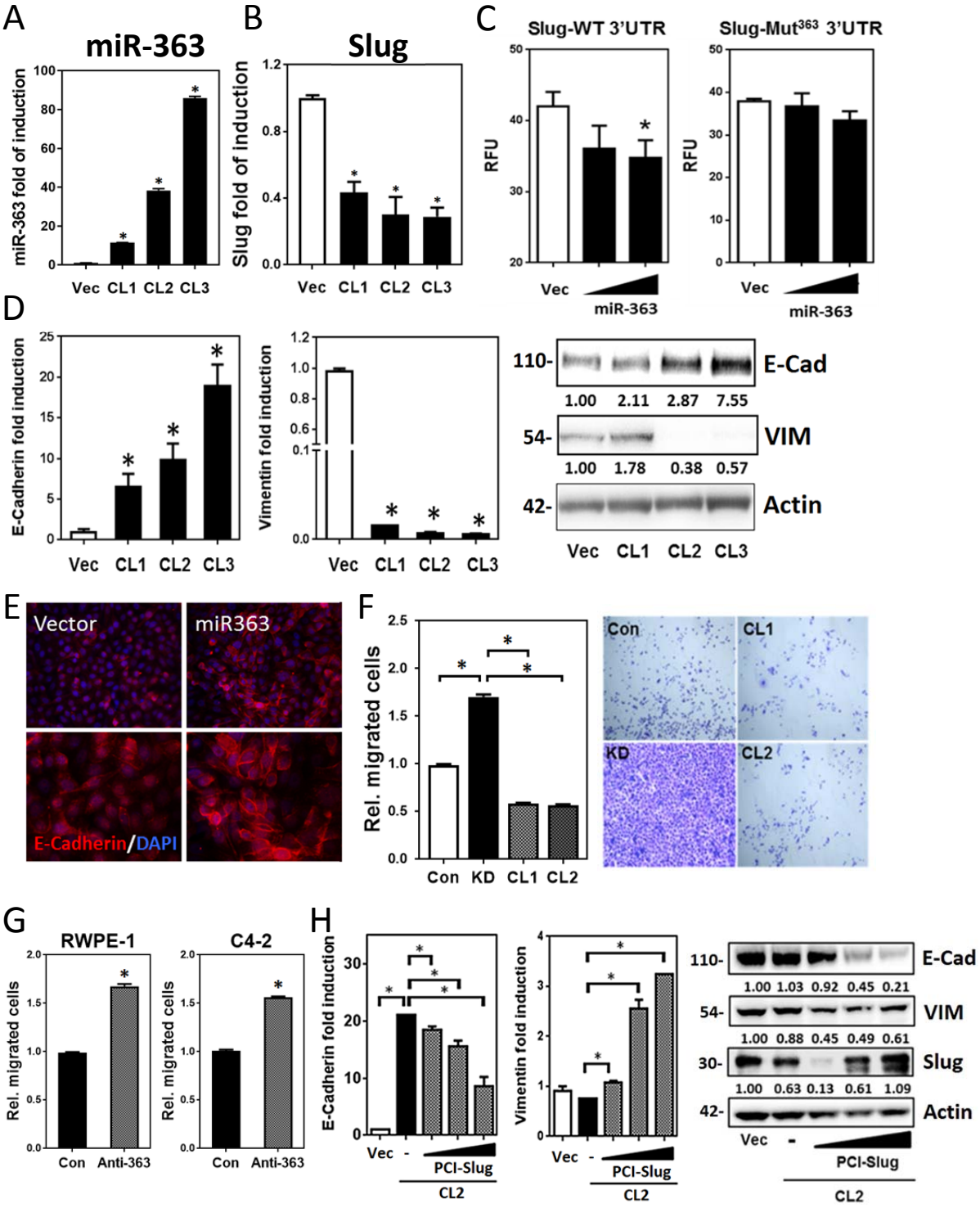
A
miR-363
miR-363 fold of induction
Vec CL1 CL2 CL3
B
Slug
Slug fold of induction
Vec CL1 CL2 CL3
C
Slug-WT 3'UTR
Slug-Mut363 3'UTR
RFU
Vec
miR-363
D
E-Cadherin fold induction
Vimentin fold induction
110-
E-Cad
1.00 2.11 2.87 7.55
54-
VIM
1.00 1.78 0.38 0.57
42-
Actin
Vec CL1 CL2 CL3
E
Vector
miR363
E-Cadherin/DAPI
F
Rel. migrated cells
Con KD CL1 CL2
Con
CL1
KD
CL2
G
RWPE-1
C4-2
Rel. migrated cells
Con Anti-363
H
E-Cadherin fold induction
Vimentin fold induction
Vec - PCI-Slug
CL2
110-
E-Cad
1.00 1.03 0.92 0.45 0.21
54-
VIM
1.00 0.88 0.45 0.49 0.61
30-
Slug
1.00 0.63 0.13 0.61 1.09
42-
Actin
Vec - PCI-Slug
CL2

Figure 3. miR-363 reverse EMT signaling via targeting Slug

(A) Elevated miR-363 levels in RWPE1-KD cells stably transfected with pCMV-miR-363 plasmid. (B) Reduction of Slug mRNA expression and protein level in RWPE1-KD cells expressing miR-363. (CL: stable clone of RWPE1-KD cells expressing miR-363) (C) Luciferase reporter assay in RWPE1-KD cells co-transfected with siCHECK2-slug-WT 3'UTR or siCHECK2-Slug Mut363 3'UTR and pCMV-miR363 or empty vector. Luciferase activity unit is plotted as Renilla to Firefly luciferase activity (RFU). Each bar represents mean ± SD of four replicated experiments. (D) Induced mRNA and protein expression of E-cadherin and Vimentin in RWPE1-KD cells expressing miR-363. (E) Immunofluorescence staining of E-cadherin protein expression in miR-363-overexpressed RWPE1-KD cells, compared to vector control. (F) Transwell migration assay in RWPE1-KD cells-expressing miR363. Transmigrated RWPE1 cells were observed by crystal violet staining and quantified at OD 555nm. Each bar represents mean ± SD of three replicated experiments. (*<0.05). (G) Transwell migration assay in RWPE1-Con and C4-2D2 cells transfected with anti-miR-363. Transmigrated cells were stained with crystal violet and quantified at OD 555nm. Each bar represents mean ± SD of three replicated experiments. (*<0.05). (H) E-cadherin and Vimentin mRNA and protein expression level after restoration of slug in RWPE1-KD cells-expressing miR363.

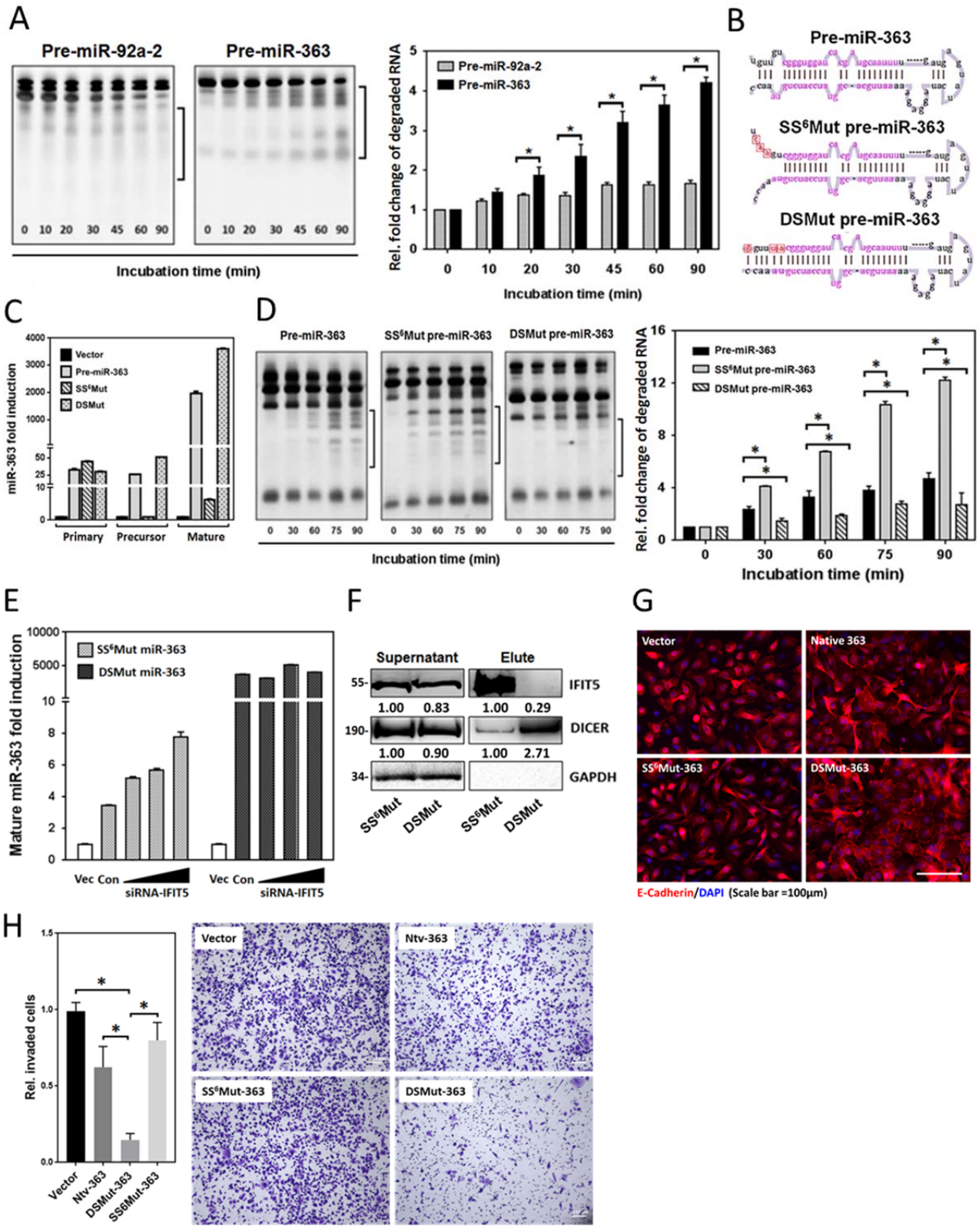
A
Pre-miR-92a-2
Pre-miR-363
0 10 20 30 45 60 90
Incubation time (min)
Rel. fold change of degraded RNA
Pre-miR-92a-2
Pre-miR-363
Incubation time (min)
B
Pre-miR-363
SS6Mut pre-miR-363
DSMut pre-miR-363
C
miR-363 fold induction
Vector
Pre-miR-363
SS6Mut
DSMut
Primary
Precursor
Mature
D
Pre-miR-363
SS6Mut pre-miR-363
DSMut pre-miR-363
0 30 60 75 90
Incubation time (min)
Rel. fold change of degraded RNA
Incubation time (min)
E
Mature miR-363 fold induction
SS6Mut miR-363
DSMut miR-363
Vec Con
siRNA-IFIT5
F
Supernatant
Elute
55-
IFIT5
1.00 0.83 1.00 0.29
190-
DICER
1.00 0.90 1.00 2.71
34-
GAPDH
SS6Mut
DSMut
G
Vector
Native 363
SS6Mut-363
DSMut-363
E-Cadherin/DAPI (Scale bar =100μm)
H
Rel. invaded cells
Vector
Ntv-363
DSMut-363
SS6Mut-363

734

735

Figure 4. IFIT5-mediated precursor miR-363 degradation in vitro.

(A) Time-dependent change of degraded pre-miR-92a-2 and pre-miR-363 fragments (bracket) after incubation with IFIT5 protein complex at 37°C normalized with 0 min. (*P<0.05) (B) Mutation of nucleotides (red box) for generating 5'-end 6 nucleotides single stranded pre-miR-363 (SS6Mut pre-miR-363) and blunt 5'-end double stranded pre-miR-363 (DSMut pre-miR-363). Both mature miR-363 and miR-363* sequence are shown in pink. (C) Expression levels of primary, precursor and mature miR-363 in LAPC4-KD cells transfected with Native, SS6Mut or DSMut pre-miR-363 plasmids for 24 hrs after normalizing with the vector control. (D) Time-dependent change of degraded native, SS6Mut and DSMut pre-miR-363 fragments (bracket) after incubation with IFIT5 protein at 37°C, each time point was normalized with 0 min. (*p<0.05) (E) Induction of mature miR-363 in cells transfected with SS6Mut pre-miR-363 or DSMut pre-miR-363 plasmids and IFIT5 siRNA after normalizing with the control vector (Vec). (Con=control siRNA). (F) Interaction between IFIT5 protein and SS6Mut or DSMut pre-miR-363 RNA molecules using RNA pull down assay. (G) Immunofluorescence staining of E-cadherin protein expression in mutant pre-miR-363-overexpressed RWPE1 cells, compared to vector control. (H)The effect of Native, DSMut-or SS6Mut-pre-miR-363 on cell invasion in PC3 cells. Cells invaded at the lower bottom at the Transwell were stained with crystal violet and counted. Each bar represents mean ± SD of nine fields of counted cell numbers. (* p<0.05)

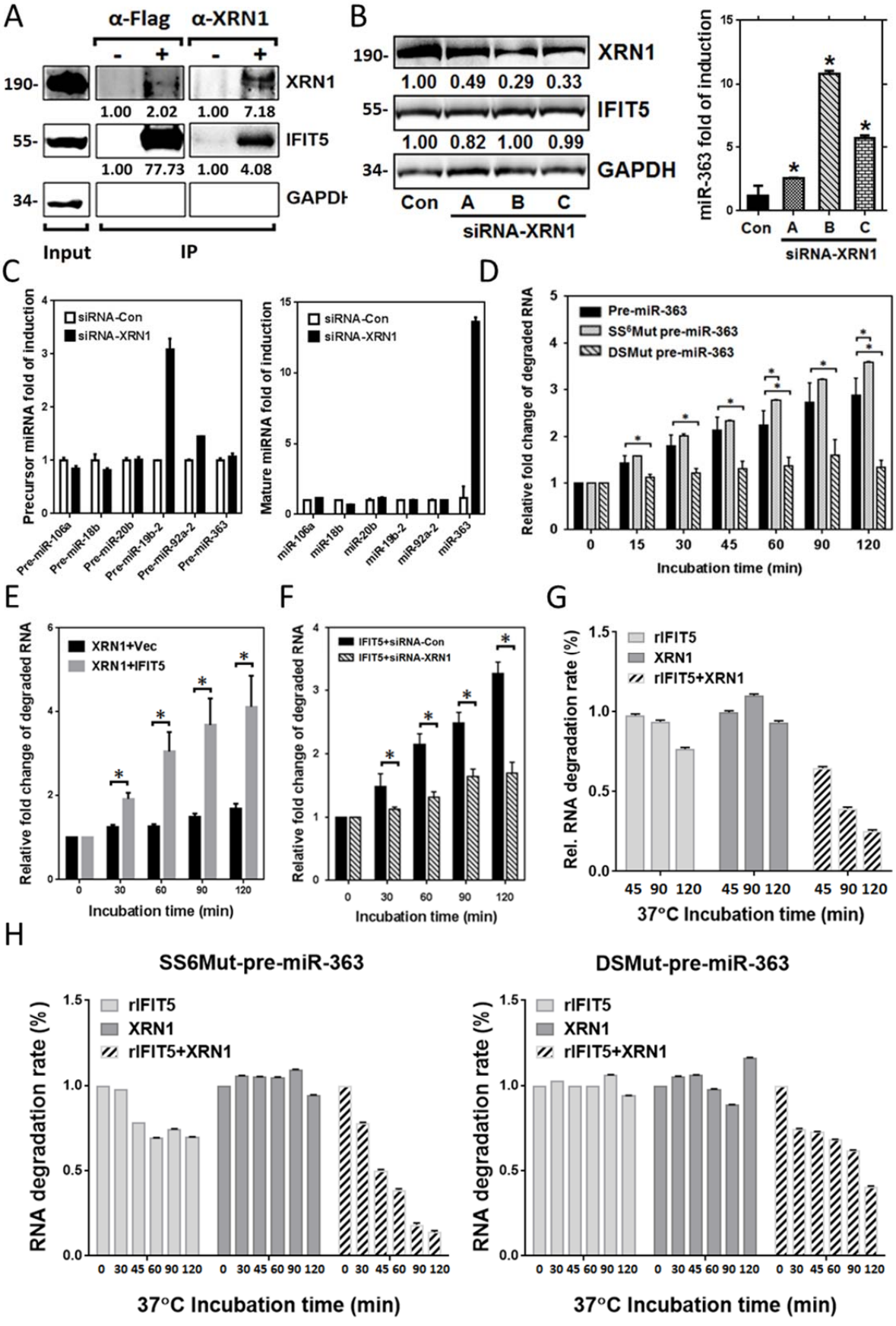
A
α-Flag
α-XRN1
XRN1
IFIT5
GAPDH
Input
IP
B
XRN1
IFIT5
GAPDH
Con
siRNA-XRN1
miR-363 fold of induction
C
siRNA-Con
siRNA-XRN1
Precursor miRNA fold of induction
Mature miRNA fold of induction
Pre-miR-106a
Pre-miR-18b
Pre-miR-20b
Pre-miR-19b-2
Pre-miR-92a-2
Pre-miR-363
miR-106a
miR-18b
miR-20b
miR-19b-2
miR-92a-2
miR-363
D
Pre-miR-363
SS⁶Mut pre-miR-363
DSMut pre-miR-363
Relative fold change of degraded RNA
Incubation time (min)
E
XRN1+Vec
XRN1+IFIT5
Relative fold change of degraded RNA
Incubation time (min)
F
IFIT5+siRNA-Con
IFIT5+siRNA-XRN1
Relative fold change of degraded RNA
Incubation time (min)
G
rIFIT5
XRN1
rIFIT5+XRN1
Rel. RNA degradation rate (%)
37°C Incubation time (min)
H
SS6Mut-pre-miR-363
DSMut-pre-miR-363
rIFIT5
XRN1
rIFIT5+XRN1
RNA degradation rate (%)
37°C Incubation time (min)

761

Figure 5. Interaction between XRN1 with IFIT5 leading to pre-miR-363 degradation in vitro.

(A) Interaction between IFIT5 and XRN1 proteins using IP by Flag and XRN1 antibodies, respectively. (B) Left: knockdown of XRN1 in LAPC4-KD cells using siRNA. Right: Induction of mature miR-363 in LAPC4-KD cells transfected with XRN1 siRNA after normalizing with the control siRNA (Con). (C) Expression levels of precursor and mature miRNAs (miR-106a, miR-18b, miR-20b, miR-19b-2, miR-92a-2 and miR-363) in XRN1-knockdown (siRNA-XRN1) LAPC4-KD cells after normalizing with the control siRNA (siRNA-Con). (D) Time-dependent change of degraded native, SS6Mut and DSMut pre-miR-363 fragments after incubation with immunoprecipitated XRN1 protein at 37°C after normalizing with 0 min. (*$p<0.05$) (E) Time-dependent change of degraded SS6Mut pre-miR-363 fragments after incubation with immunoprecipitated-XRN1 alone (XRN1+Vec) or XRN1-IFIT5 complex (XRN1+IFIT5) at 37°C after normalizing with 0 min. (*$p<0.05$) (F) Time-dependent change of degraded SS6Mut pre-miR-363 after incubation with the immunocomplex derived from cells transfected with IFIT5 and control siRNA (IFIT5+siRNA-Con) or XRN1 siRNA (IFIT5+siRNA-XRN1) at 37°C after normalizing with 0 min. (*$p<0.05$) (G) Degradation of native pre-miR-363 after incubation with recombinant IFIT5 protein (rIFIT5), XRN1 enzyme (XRN1) or combination of XRN1 and rIFIT5 at 37°C after normalizing with 0 min. (H) Degradation of SS6Mut-or DSMut- pre-miR-363 after incubation with rIFIT5, XRN1 or combination of XRN1 and rIFIT5 at 37°C after normalizing with 0 min.

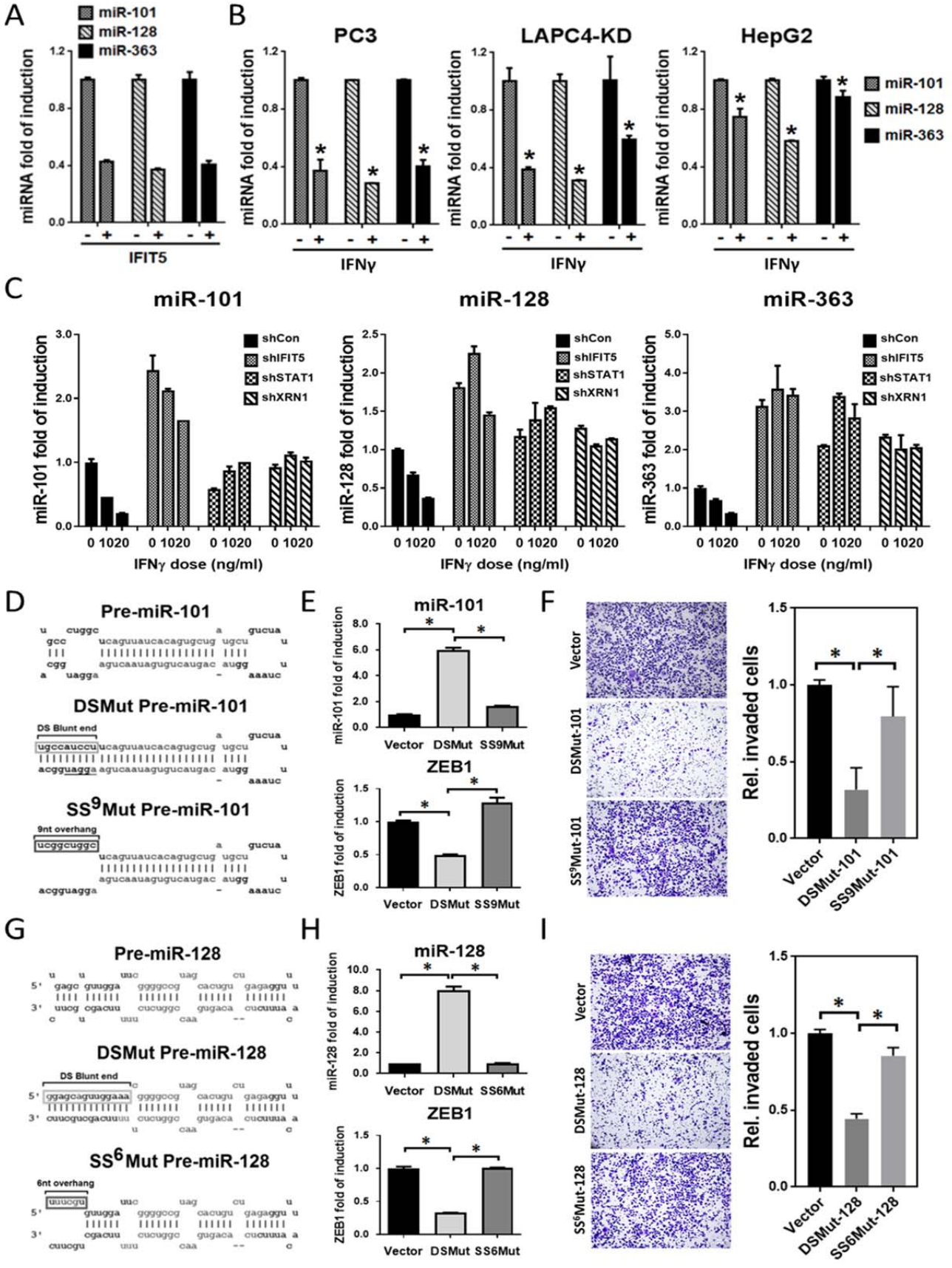
A
miR-101
miR-128
miR-363
miRNA fold of induction
IFIT5
B
PC3
LAPC4-KD
HepG2
IFNγ
C
miR-101
miR-128
miR-363
shCon
shIFIT5
shSTAT1
shXRN1
IFNγ dose (ng/ml)
D
Pre-miR-101
DSMut Pre-miR-101
DS Blunt end
SS9Mut Pre-miR-101
9nt overhang
E
ZEB1
Vector
DSMut
SS9Mut
F
Rel. invaded cells
DSMut-101
SS9Mut-101
G
Pre-miR-128
DSMut Pre-miR-128
SS6Mut Pre-miR-128
6nt overhang
H
SS6Mut
I
DSMut-128
SS6Mut-128

785

Figure 6. The impact of IFIT5-XRN1 mediated precursor miRNA degradation on EMT. (A) Expression level of mature miR-101, miR-128 and miR-363 in IFIT5-overexpressed PC3 cells. (B) Expression level of miR-101, miR-128 and miR-363 in PC3, LAPC4-KD and HepG2 cells treated with IFNγ(+), compared with control vector (-). (C) Expression level of miR-101, miR-128 and miR-363 in PC3 cells treated with 0, 10 and 20 ng/ml dose of IFNγ after knockdown of IFIT5 (shIFIT5), STAT1 (shSTAT1) or XRN1 (shXRN1), compared to vector control (shCon). (D) Mutation of nucleotides (box) for generating blunt 5'-end double stranded pre-miR-101 (DSMut pre-miR-101) and 5'-end 9 nucleotides single stranded pre-miR-101 (SS9Mut pre-miR-101). Both mature miR-101 and miR-101* sequence are shown in lighter gray. (E) The effect of DSMut or SS9Mut pre-miR-101 on the expression level of mature miR-101 and ZEB1 mRNA (* $p<0.05$). (F) The effect of DSMut or SS9Mut pre-miR-101 on the cell invasion in PC3 cells. Cells invaded at the lower bottom at the Transwell were stained with crystal violet and counted. Each bar represents mean ± SD of nine fields of counted cell numbers. (* $p<0.05$). (G) Mutation of nucleotides (box) for generating blunt 5'-end double stranded pre-miR-128 (DSMut pre-miR-128) and 5'-end 6 nucleotides single stranded pre-miR-128 (SS6Mut pre-miR-128). Both mature miR-128 and miR-128* sequence are shown in lighter gray. (H) The effect of DSMut or SS6Mut pre-miR-128 on the expression level of mature miR-128 and ZEB1 mRNA (* $p<0.05$). (I) The effect of DSMut or SS6Mut pre-miR-128 on the cell invasion of PC3 cells. Cells invaded at the lower bottom at the Transwell were stained with crystal violet and counted. Each bar represents mean ± SD of nine fields of counted cell numbers. (* $p<0.05$).

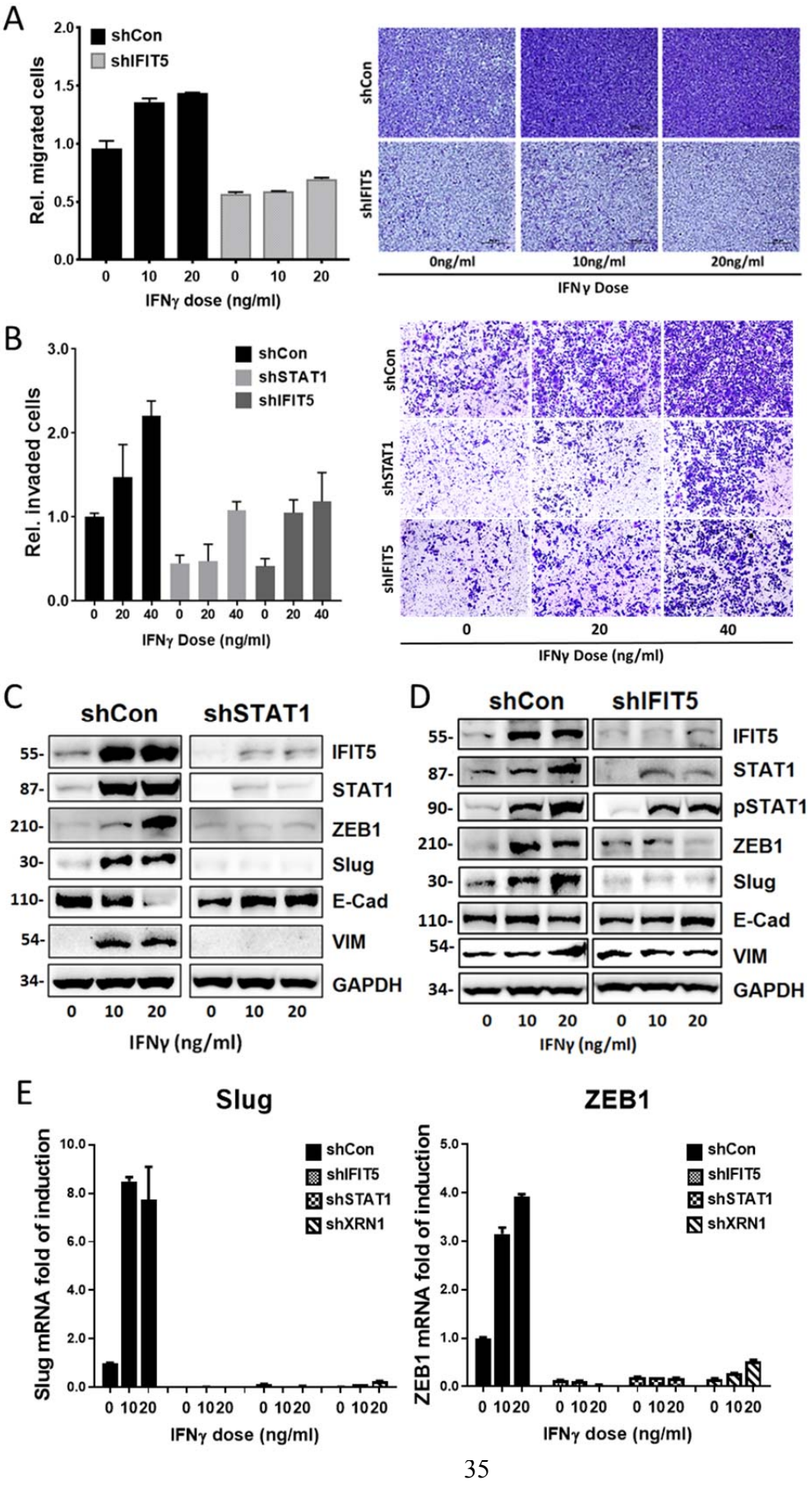
A
shCon
shIFIT5
Rel. migrated cells
IFNγ dose (ng/ml)
shCon
shIFIT5
0ng/ml
10ng/ml
20ng/ml
IFNγ Dose
B
shCon
shSTAT1
shIFIT5
Rel. invaded cells
IFNγ Dose (ng/ml)
shCon
shSTAT1
shIFIT5
IFNγ Dose (ng/ml)
C
shCon
shSTAT1
IFIT5
STAT1
ZEB1
Slug
E-Cad
VIM
GAPDH
IFNγ (ng/ml)
D
shCon
shIFIT5
IFIT5
STAT1
pSTAT1
ZEB1
Slug
E-Cad
VIM
GAPDH
IFNγ (ng/ml)
E
Slug
ZEB1
shCon
shIFIT5
shSTAT1
shXRN1
Slug mRNA fold of induction
ZEB1 mRNA fold of induction
IFNγ dose (ng/ml)

Figure 7. IFNγ elicits its impact on EMT via activating IFIT5-XRN1 mediated miRNA turnover through STAT1 signaling pathway

(A) Transwell migration of IFIT5-knockdown (shIFIT5) PC3 cells after treatment of IFNγ for 48hrs, compared to vector control (shCon). Migrated cells were stained with crystal violet and quantified at OD 555nm. Each bar represents mean ± SD of three replicated experiments. (* $p<0.05$, NS=no significance). (B) Transwell invasion of STAT1- or IFIT5-knockdown (shSTAT1, shIFIT5) PC3 cells after treatment of IFNγ (0, 20, and 40 ng/ml) for 48hrs, compared to control vector (shCon). Cells invaded at the lower bottom of Transwell were stained with crystal violet and counted. Each bar represents mean ± SD of counted cell numbers from nine fields. (* $p<0.05$) (Scale bar =100μm). (C-D) Induction of IFIT5, E-cadherin and mesenchymal factors (ZEB1, Slug and Vimentin) in STAT1- or IFIT5-knockdown (shSTAT1 or shIFIT5) PC3 cell lines in response to IFNγ treatment, compared to PC3 cells with control vector (shCon). (E) Induction level of Slug and ZEB1 mRNA in PC3 cells treated with 0, 10 and 20 ng/ml dose of IFNγ after knockdown of IFIT5 (shIFIT5), STAT1 (shSTAT1) or XRN1 (shXRN1), compared to vector control (shCon).

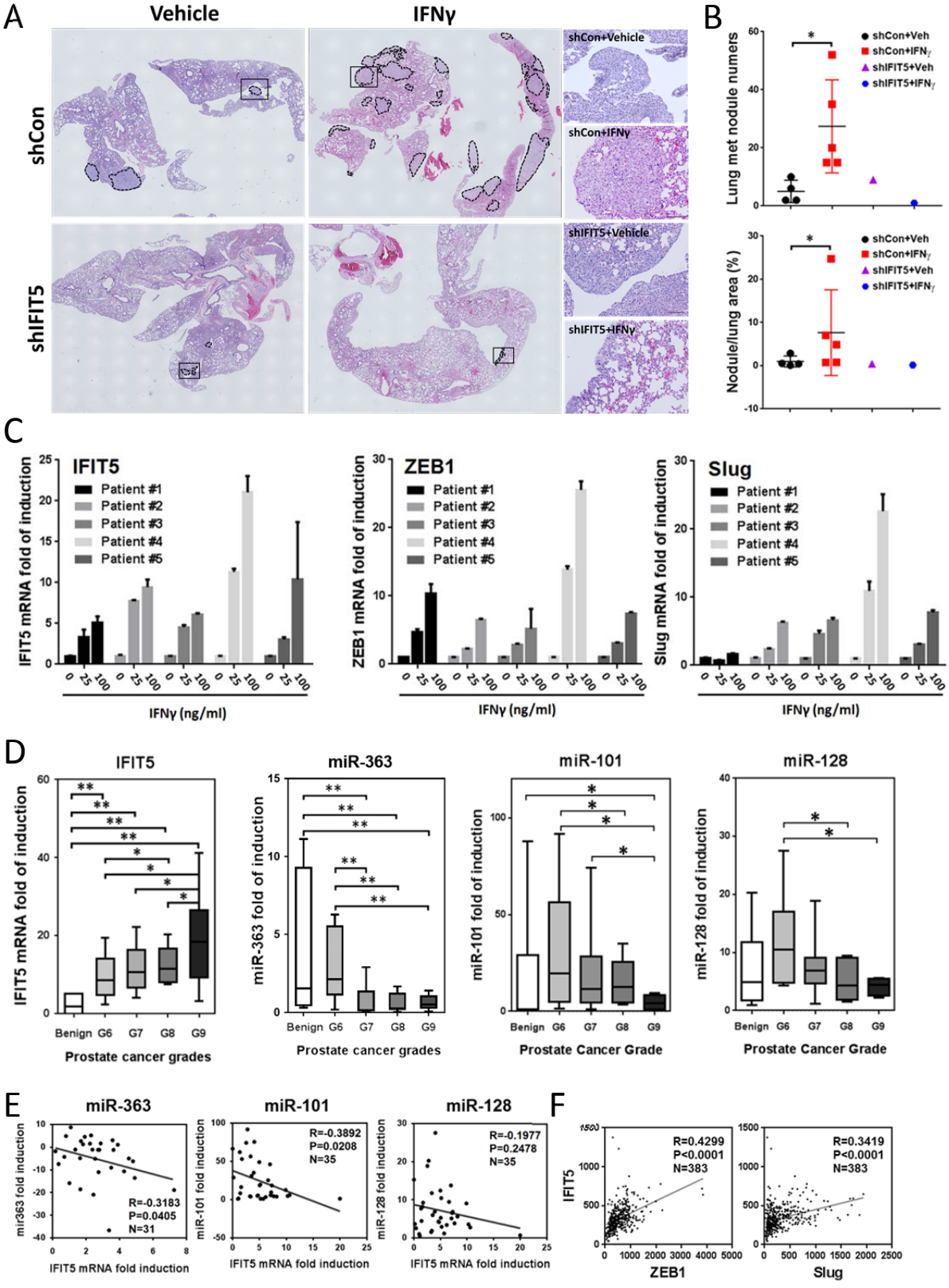
A
Vehicle
IFNγ
shCon
shIFIT5
shCon+Vehicle
shCon+IFNγ
shIFIT5+Vehicle
shIFIT5+IFNγ
B
Lung met nodule numers
Nodule/lung area (%)
shCon+Veh
shCon+IFNγ
shIFIT5+Veh
shIFIT5+IFNγ
C
IFIT5
ZEB1
Slug
Patient #1
Patient #2
Patient #3
Patient #4
Patient #5
IFIT5 mRNA fold of induction
ZEB1 mRNA fold of induction
Slug mRNA fold of induction
IFNγ (ng/ml)
D
IFIT5
miR-363
miR-101
miR-128
IFIT5 mRNA fold of induction
miR-363 fold of induction
miR-101 fold of induction
miR-128 fold of induction
Benign G6 G7 G8 G9
Prostate cancer grades
Prostate Cancer Grade
E
miR-363
miR-101
miR-128
mir363 fold induction
miR-101 fold induction
miR-128 fold induction
R=-0.3183
P=0.0405
N=31
R=-0.3892
P=0.0208
N=35
R=-0.1977
P=0.2478
N=35
IFIT5 mRNA fold induction
F
IFIT5
R=0.4299
P<0.0001
N=383
R=0.3419
P<0.0001
N=383
ZEB1
Slug

833

834

G

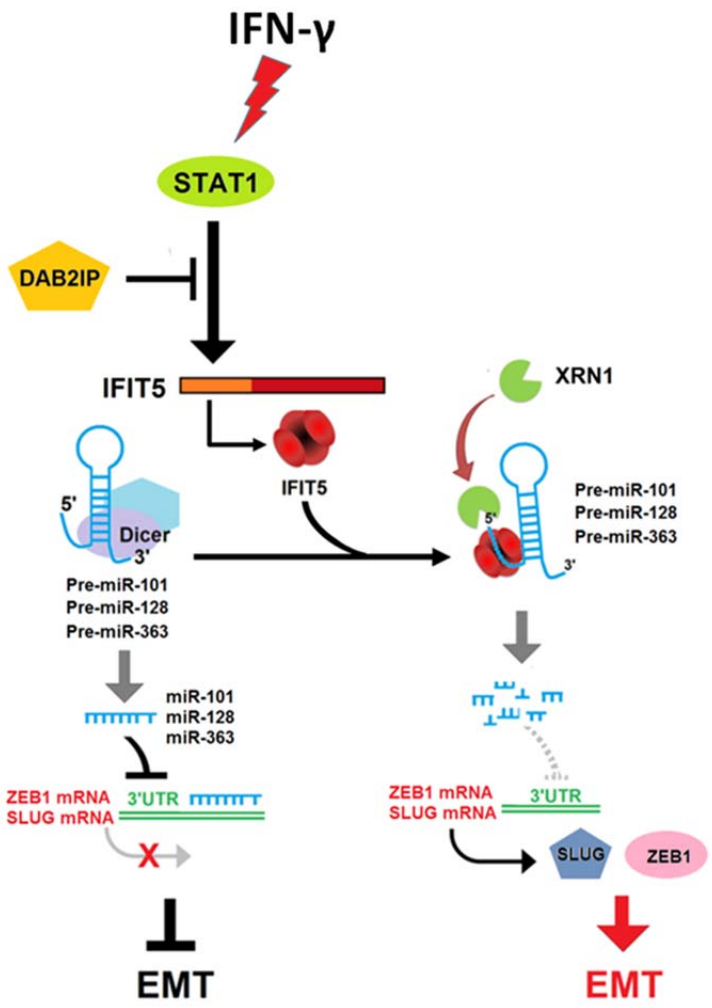
IFN-γ
STAT1
DAB2IP
IFIT5
IFIT5
5'
Dicer
3'
Pre-miR-101
Pre-miR-128
Pre-miR-363
miR-101
miR-128
miR-363
ZEB1 mRNA
SLUG mRNA
3'UTR
X
EMT
XRN1
Pre-miR-101
Pre-miR-128
Pre-miR-363
5'
3'
ZEB1 mRNA
SLUG mRNA
3'UTR
SLUG
ZEB1
EMT

Figure 8. The effect of IFIT5-mediated miRNA degradation on EMT and its clinical correlation in PCa.

(A) The incidence of lung metastasis, tumor nodule number and size in SCID mice receiving intravenous injection of IFIT5-knockdown PC3 cells (shIFIT5) pretreated with vehicle (Veh, PBS) or IFNγ (20 ng/ml) for 48hrs, compared to PC3 cells transfected with control vector (shCon). (B) HE staining of lung tissue derived from mice receiving tail vein intravenous injection of IFIT5-knockdown PC3 cells (PC3-shIFIT5) pretreated with vehicle (Veh, PBS) or IFNγ (20 ng/ml), compared to PC3 cells transfected with control vector (shCon). The black dotted line-circles region indicate the presence metastatic nodules observed at lung parenchyma. Representative tumor nodules from each group are shown at right side panels (scale bar =100 μm). (C) Comparison of tumor nodule numbers and comparative area ratio in the lung parenchyma among each group. (D) Induction level of IFIT5, ZEB1, and Slug mRNA expression in ex vivo culture of human PCa specimens treated with IFNγ (0, 25 and 100 ng/ml) for 48 hrs. (E) Relative expression of IFIT5 mRNA and mature miR-363, miR-101 and miR-128 level in human PCa specimens derived from different grades including benign (N=10), G6 (N=9), G7(N=9), G8(N=6) and G9(N=7) (*$p<0.05$, **$p<0.0001$). (F) Clinical correlation of miR-363, miR-101 and miR-128 with IFIT5 mRNA expression in human PCa specimens graded from benign, G6 to G9. (G) Clinical correlation between IFIT5 and ZEB1 or Slug mRNA level in PCa from TCGA PCa dataset. (H) Schematic representing IFN induced IFIT5-mediated precursor microRNA degradation leading to EMT in cancer.

SUPPLEMENTAL FIGURES AND FIGURE LEGENDS

Figure S1.

(A) Profile of miRNA expression in RWPE1-KD cells compared with RWPE1-Con cells. (B) Relative fold change of each miRNA from microarray screening (miScript miRNA PCR Array Human Prostate Cancer, QIAGEN). Green and red indicate decreased and increased fold change in RWPE1-KD cells after normalizing with RWPE1-Con cells, respectively. (C) The expression levels of mature miR-363 in DAB2IP-KD renal cell lines (786-O and HK2) after normalizing with the vector control (Con). (D) Induction of mature miR-363 by ectopic expression of DAB2IP in HEK293 cells. (E) Expression levels of precursor and mature miRNAs (miR-106a, iR-18b, miR-20b, miR-19b-2, miR-92a-2 and miR-363) in DAB2IP-expressing HEK293D cells after normalizing with HEK293 cells.

Figure S2

(A) Relative change of IFIT5 mRNA and protein level in pairs of DAB2IP-positive and –negative prostate cells (LAPC4, RWPE1 and C4-2). (B-C) Suppression of IFIT5 protein expression by ectopic expression of DAB2IP in LNCaP and HEK293 cell lines after normalizing with the control vector (Vec). (D) Induction of mature miR-363 in LAPC4-KD cells transfected with IFIT5 siRNAs compared with control siRNA (Con). (E) Induction of mature miR-363 in LAPC4-KD and RWPE1-KD cells by IFIT5 siRNA knockdown after normalizing with the control siRNA (Con). (F) Expression levels of mature miRNAs (miR-106a, miR-18b, miR-20b, miR-19b-2, miR-92a-2 and miR-363) in IFIT5-KD (siRNA-IFIT5/+) LNCaP cells compared with the control siRNA (siRNA-Con/-). (G) Expression levels of precursor miRNAs (miR-106a, miR-18b, miR-20b, miR-19b-2, miR-92a-2 and miR-363) in IFIT5-KD (siRNA-IFIT5) LAPC4-KD, C4-2Neo, RWPE1-KD and LNCaP cells after normalizing with the control siRNA (siRNA-Con). (H-I) Left: Induction of IFIT5 protein and mRNA level in 786O and HepG2 cells treated with IFNγ (10ng/ml) for 48 hrs. Right panel: Expression levels of mature miRNAs (miR-106a, miR-18b, miR-20b, miR-19b-2, miR-92a-2 and miR-363) in 786O and HepG2 cells treated with IFNγ (10ng/ml) for 48 hrs.

Figure S3

(A) Reduction of Slug/SNAI2 mRNA levels in miR-363-expressing LAPC4-KD cells after normalizing with the control vector (Vec). (*p<0.05, CL: miR-363 expressing stable clone) (B) Luciferase reporter activities in LAPC4-KD cells co-transfected with siCHECK2-Slug-WT 3'UTR or -Slug Mut363 3'UTR and pCMV-miR363 or control vector. (RFU=Renilla to Firefly luciferase activity, each bar represents mean ± SD of four replicated experiments. * p<0.05) (C) Expression levels of E-cadherin and Vimentin mRNA and protein level in miR-363-expressing LAPC4-KD cell. (D) Left and right: The effect of miR-363 on cell migration of GFP–expressing LAPC4-KD cells. Migrated GFP-positive cells were observed under microscope and migrated cells were stained with crystal violet and quantified at O.D. 555nm. (Each bar represents mean ± SD of three replicated experiments. *p<0.05). Middle: miR-363 expression level in LAPC4-KD cells migrated to the lower chamber, compared to cells stay at upper chamber. (KD: DAB2IP-knockdown, CL: miR-363 expressing stable clone of LAPC4-KD cells) (E) The effect of Slug on the expression levels of E-cadherin and Vimentin mRNA and protein in miR-363-expressing LAPC4-KD cells (CL3) after normalizing with the control vector (Con). (*P<0.05).

Figure S4

(A) The expression level of miR-363 and IFIT5 protein among prostate (LAPC4), liver (HepG2) and kidney (293T, HK2 and 786O) cancer cell lines. (B) Induction of mature miR-363 levels in IFIT5-shRNA knockdown (shIFIT5, +) HepG2, 293T and 786O cell lines, compared to the control shRNA (-). (C, F, I) Overexpression of miR-363 in HepG2, 293T and 786O cell lines. (D, G, J) The impact of miR-363 on the mRNA and protein level of E-cadherin, Slug and Vimentin in HepG2, 293T and 786O cell lines transfected with pCMV-miR-363 (363), compared to control vector (Vec). (E, H, K) Transwell migration of miR-363 expressing HepG2, 293T and 786O cells (363), compared to the cells with control vector (Vec).

Figure S5

(A) Upper: Immunoprecipitation (IP) of ectopic expressed IFIT5 protein subjected to in vitro RNA degradation assay. Middle panel: Gel electrophoresis of Native pre-miR-363 fragments after incubation with IFIT5 protein (IP) or elution buffer at 37°C. Lower: Time-dependent change of degraded pre-miR-363 fragments (bracket) after normalized with 0 min. (B) Expression levels of primary, precursor and mature miR-363 in RWPE1-KD cells transfected with native, SS6Mut or DSMut pre-miR-363 plasmids for 24 hrs and normalized with the control vector (Vec). (C) Expression levels of mature miR-363 in LAPC4-KD cells transfected with SS6Mut or DSMut pre-miR-363 plasmids for 24 hrs and normalized with the control vector (Vec). (D) The effect of SS6Mut and DSMut pre-miR-363 on the expression levels of mature E-cadherin, Vimentin and Slug mRNA in LAPC4-KD cells after normalizing with the control vector. (E) The effect of SS6Mut or DSMut pre-miR-363 on cell migration in LAPC4-KD cells. Migrated cells were stained with crystal violet and quantified at OD 555nm. Each bar represents mean ± SD of three replicated experiments. (* $p<0.05$, NS=no significance) (F) Upper panel: predicted structure and sequence of pre-miR-92a-2. Middle panel: mutation of nucleotides (red box) for generating single nucleotide overhanging structure of pre-miR-92a-2 (SS1Mut). Lower panel: interaction between IFIT5 protein and pre-miR-92a-2 or SS1Mut pre-miR-92a-2 RNA molecules using RNA pull down assay. (G) Time-dependent change of degraded pre-miR-92a-2 and SS1Mut pre-miR-92a-2 after incubating with IFIT5 protein complex at 37°C normalized with 0 min. (*$P<0.05$).

Figure S6

(A) Induction of miR-363 expression in LAPC4-KD cells transfected with XRN1 siRNA-B and compared with the control siRNA (Con). (B) Left panel: IP of endogenous XRN1 protein subjected to in vitro RNA degradation assay. Right panel: Time-dependent change of degraded native, SS6Mut and DSMut pre-miR-363 RNA molecules (bracket) after incubation with IP-XRN1 protein at 37°C, each time point was normalized with 0 min. (C) Left panel: Western blot from Vector or IFIT5-transfected LAPC4-Con cells. Right panel: Time-dependent change of degraded SS6Mut pre-miR-363 fragments in the presence of XRN1 alone (XRN1+Vector) or XRN1-IFIT5 complex (XRN1+IFIT5) at 37°C. (D) Left panel: western blot from IFIT5-expressing LAPC4-Con cells transfected with control or XRN1 siRNA. Right panel: Time-dependent change of degraded SS6Mut pre-miR-363 fragments in the presence of XRN1-IFIT5 complex derived from IFIT5 w/ siRNA-Con or IFIT5 w/ siRNA-XRN1 at 37°C. (E) In vitro miRNA degradation of native pre-miR-363 after incubating with recombinant IFIT5 protein (rIFIT5), XRN1 enzyme (XRN1) or combination of XRN1 and rIFIT5 at 37°C for 45, 90 and 120 min. (F) In vitro miRNA degradation of SS6Mut- or DSMut-pre-miR-363 after incubating with rIFIT5, XRN1 or combination of XRN1 and rIFIT5 at 37°C for 0, 30, 45, 60, 90, and 120 min.

Figure S7

(A) Expression level of mature miR-101, miR-128 and miR-363 in IFIT5-shRNA knockdown LAPC4-KD. (B) Dose-dependent recovery of mature miR-363, miR-101 and miR-128 expression in IFIT5-expressing LAPC4-KD cells transfected with XRN1 siRNA after normalizing with the control vector (Con: control siRNA, *$p<0.05$).(C) Expression level of mature miR-101, miR-128 and miR-363 in DAB2IP-overexpressing PC3 cell lines treated with IFNγ (0, 10 and 20ng/ml) for 48hrs (*$P<0.05$). (D) Upper: Expression of ZEB1 mRNA level in PC3 cells overexpressed with miR-101 or miR-128, compared to vector control (miRVec). Lower: Matched sequence paired between the seed region of miR-101 or miR-128 and the 3'UTR of ZEB1 mRNA. (E) Left and Middle panel: The effect of DSMut and SS9Mut pre-miR-101 on the expression levels of mature miR-101 and ZEB1 mRNA level in LAPC4-KD cells after normalizing with the control vector. Right panel: The effect of DSMut and SS9Mut pre-miR-101 on cell migration in LAPC4-KD cells. Migrated cells were stained with crystal violet and quantified at OD 555nm. Each bar represents mean ± SD of three replicated experiments. (* $p<0.05$, NS=no significance). (F) Left and Middle panel: The effect of DSMut and SS6Mut pre-miR-128 on the expression levels of mature miR-128 and ZEB1 mRNA level in LAPC4-KD cells after normalizing with the control vector. Right panel: The effect of DSMut and SS6Mut pre-miR-128 on cell migration in LAPC4-KD cells. Migrated cells were stained with crystal violet and quantified at OD 555nm. Each bar represents mean ± SD of three replicated experiments. (* $p<0.05$, NS=no significance) (G) Expression of miR-200 family members in PC3 cells treated with IFNγ (Left panel) or knockdown with IFIT5 (right panel).

Figure S8

(A) Western blot demonstrating the knockdown of IFIT5 or STAT1 (+) in PC3 cells, compared to control shRNA (-). (B) Transwell migration of STAT1-shRNA knockdown (shSTAT1) PC3 cells after 48 hrs treatment of IFNγ, compared to shCon. Migrated cells were stained with crystal violet and quantified at OD 555nm. Each bar represents mean ± SD of three replicated experiments. (* $p<0.05$, NS=no significance) (C) The effect of IFNγ on Slug and ZEB1 mRNA expression level in miR-101, miR-128 or miR-363-overexpressing cells. (D) Cell proliferation rate of PC3 cells treated with different dose of IFNγ for 24, 48 and 72 hrs.

Figure S9

(A) Induction level of Vimentin mRNA expression in ex vivo culture of human PCa specimens treated with IFNγ (0, 25 and 100 ng/ml) for 48hrs. (B) Induced relative fold change of miR-128, miR-101 and miR-363 expression in ex vivo culture of human PCa specimens treated with IFNγ for 48hrs. (C) Relative induction of miR-92a-2 and miR-19b-2 in human PCa specimens derived from different grades including benign (N=10), G6 (N=9), G7(N=9), G8(N=6) and G9(N=7) (*$p<0.05$, **$p<0.0001$). (D) Clinical correlation between IFIT5 and Vimentin (VIM) in PCa from TCGA PCa dataset. (E) Clinical correlation between IFIT5 and ZEB1 or Slug in renal cancer from TCGA renal cell carcinoma dataset. (F) Clinical correlation between IFIT5 and ZEB1 or Slug in liver cancer from TCGA Hepatocellular carcinoma dataset.

Figure S1

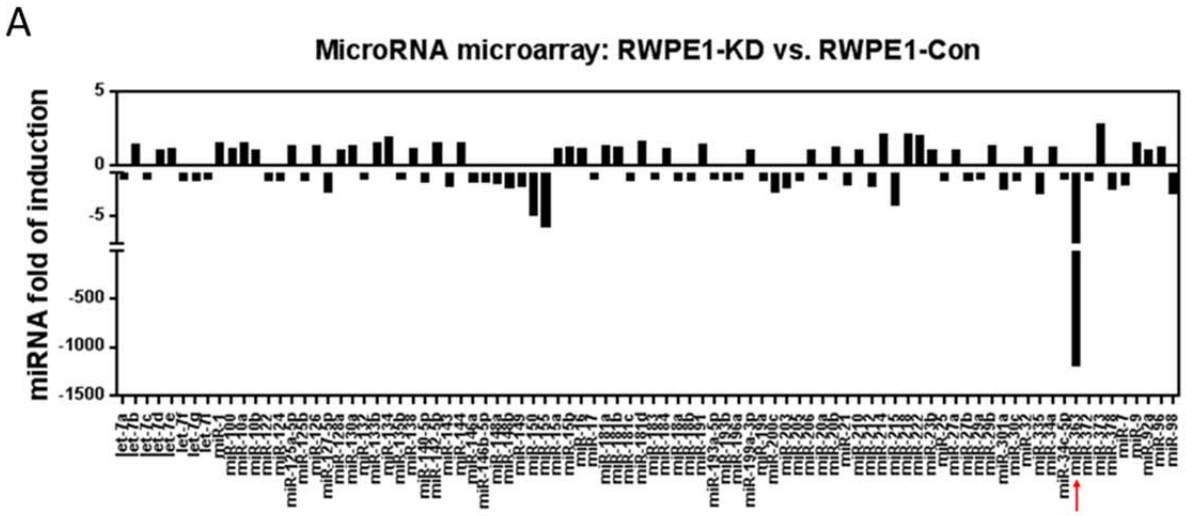

B

microRNA ↓	RWPE1-KD/Con	microRNA ↑	RWPE1-KD/Con
miR-363	-1176.27	let-7d	1.07
miR-155	-6.06	miR-128a	1.07
miR-150	-4.92	miR-206	1.07
miR-215	-3.73	miR-210	1.07
miR-335	-2.64	miR-23b	1.07
miR-98	-2.64	miR-92a	1.07
miR-127-5p	-2.46	let-7e	1.15
miR-200c	-2.46	miR-100	1.15
miR-301a	-2.14	miR-138	1.15
miR-378	-2.14	miR-15a	1.15
miR-148b	-2	miR-16	1.15
miR-203	-2	miR-184	1.15
miR-212	-1.87	miR-15b	1.23
miR-143	-1.74	miR-181b	1.23
miR-149	-1.74	miR-20b	1.23
miR-21	-1.62	miR-32	1.23
miR-7	-1.62	miR-34a	1.23
miR-148a	-1.52	miR-96	1.23
miR-140-5p	-1.41	miR-125a-5p	1.32
miR-146a	-1.41	miR-126	1.32
miR-146b-5p	-1.41	miR-130a	1.32
let-7f	-1.23	miR-181a	1.32
miR-122	-1.23	miR-29b	1.32
miR-18a	-1.23	let-7b	1.41
miR-193b	-1.23	miR-191	1.41
miR-372	-1.23	miR-1	1.52
let-7g	-1.15	miR-10a	1.52
miR-124	-1.15	miR-133b	1.52
miR-125b	-1.15	miR-142-5p	1.52
miR-181c	-1.15	miR-144	1.52
miR-18b	-1.15	miR-9	1.52
miR-19a	-1.15	miR-181d	1.62
miR-205	-1.15	miR-134	1.87
miR-25	-1.15	miR-222	2
miR-27b	-1.15	miR-214	2.14
miR-30c	-1.15	miR-218	2.14
		miR-373	2.83

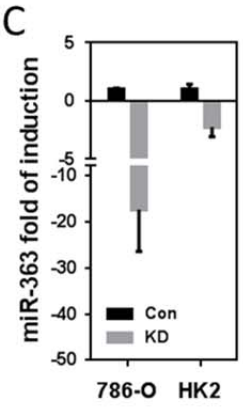

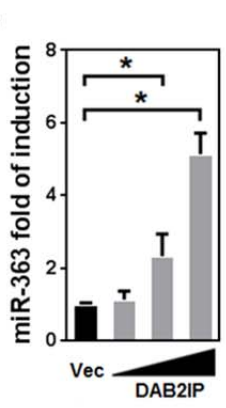

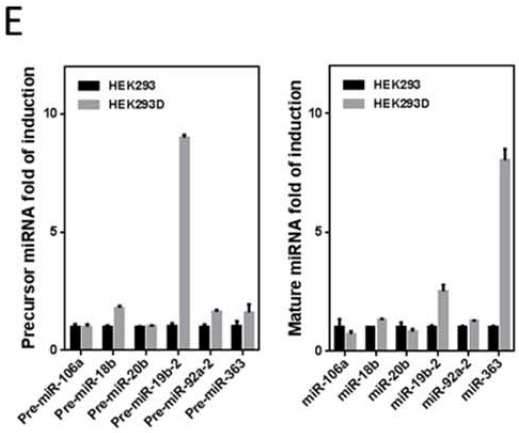

Figure S2

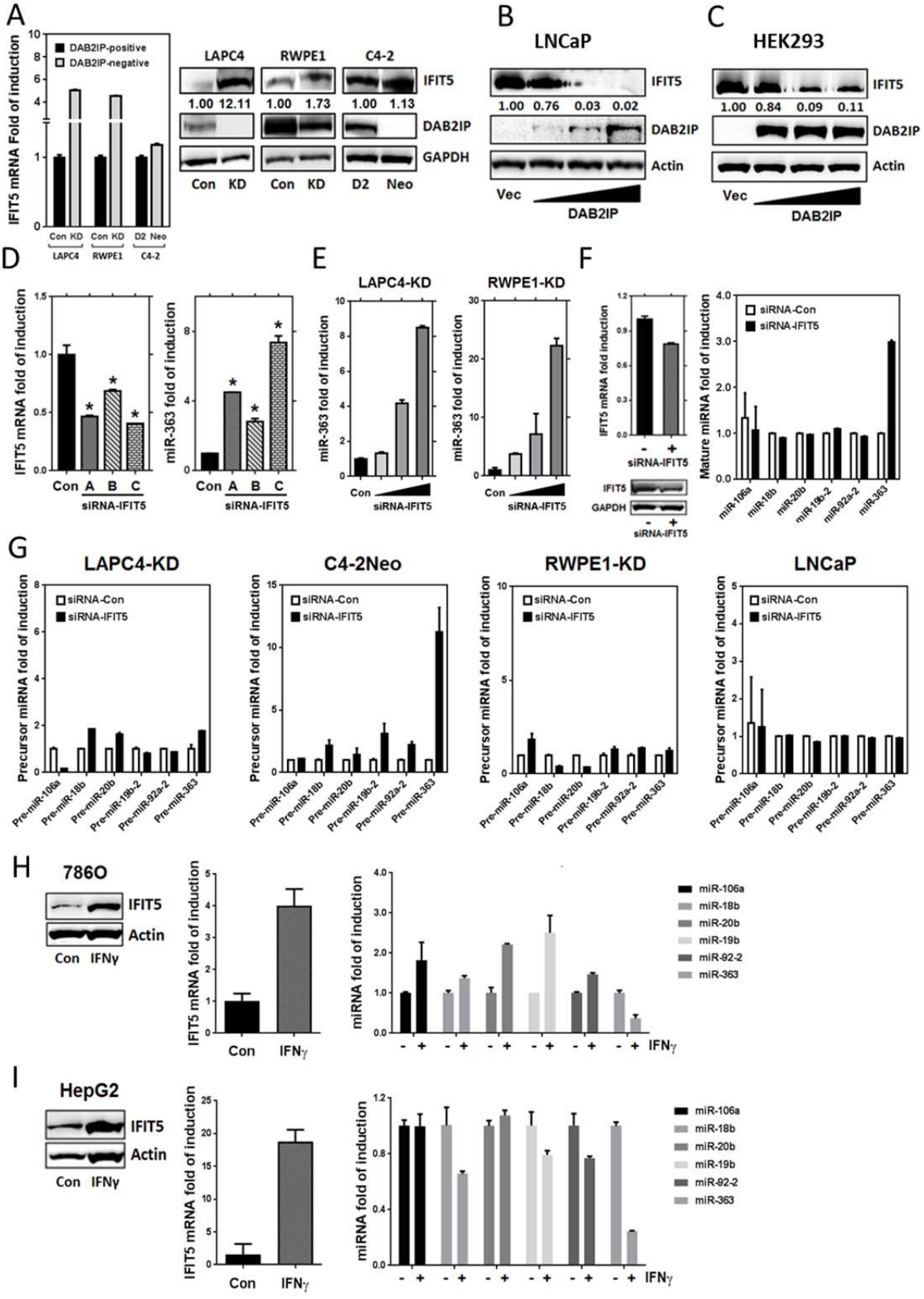
A
IFIT5 mRNA Fold of induction
DAB2IP-positive
DAB2IP-negative
Con KD Con KD D2 Neo
LAPC4 RWPE1 C4-2
LAPC4 RWPE1 C4-2
1.00 12.11 1.00 1.73 1.00 1.13
IFIT5
DAB2IP
GAPDH
Con KD Con KD D2 Neo
B
LNCaP
1.00 0.76 0.03 0.02
IFIT5
DAB2IP
Actin
Vec
DAB2IP
C
HEK293
1.00 0.84 0.09 0.11
IFIT5
DAB2IP
Actin
Vec
DAB2IP
D
IFIT5 mRNA fold of induction
Con A B C
siRNA-IFIT5
miR-363 fold of induction
Con A B C
siRNA-IFIT5
E
LAPC4-KD
miR-363 fold of induction
Con
siRNA-IFIT5
RWPE1-KD
miR-363 fold of induction
Con
siRNA-IFIT5
F
IFIT5 mRNA fold induction
- +
siRNA-IFIT5
IFIT5
GAPDH
- +
siRNA-IFIT5
Mature miRNA fold of induction
siRNA-Con
siRNA-IFIT5
miR-106a
miR-18b
miR-20b
miR-19b-2
miR-92a-2
miR-363
G
LAPC4-KD
C4-2Neo
RWPE1-KD
LNCaP
Precursor miRNA fold of induction
siRNA-Con
siRNA-IFIT5
Pre-miR-106a
Pre-miR-18b
Pre-miR-20b
Pre-miR-19b-2
Pre-miR-92a-2
Pre-miR-363
H
786O
IFIT5
Actin
Con IFNγ
IFIT5 mRNA fold of induction
Con IFNγ
miRNA fold of induction
miR-106a
miR-18b
miR-20b
miR-19b
miR-92-2
miR-363
- + - + - + - + - + - + IFNγ
I
HepG2
IFIT5
Actin
Con IFNγ
IFIT5 mRNA fold of induction
Con IFNγ
miRNA fold of induction
miR-106a
miR-18b
miR-20b
miR-19b
miR-92-2
miR-363
- + - + - + - + - + - + IFNγ

Figure S3

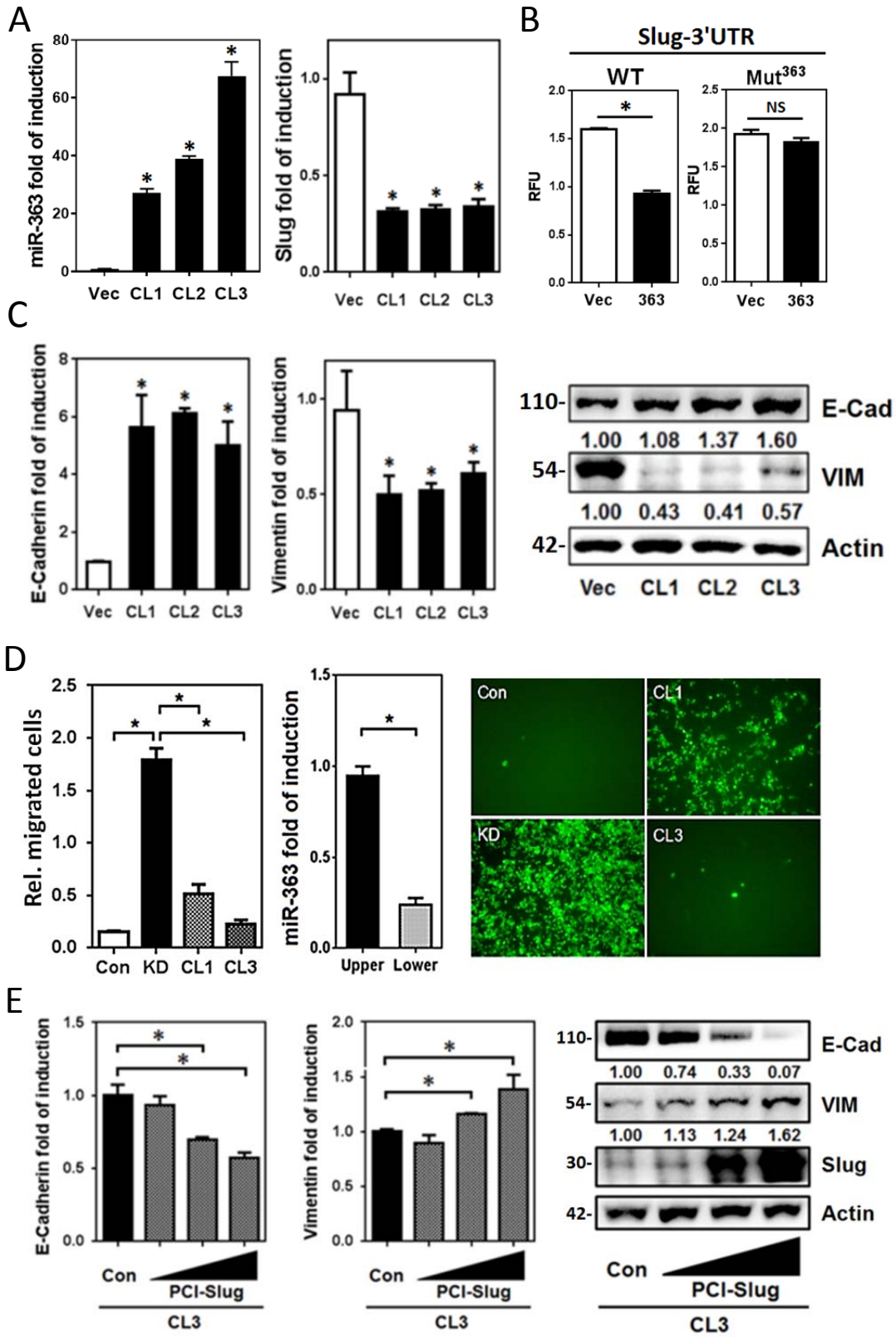
A
miR-363 fold of induction
Vec CL1 CL2 CL3
Slug fold of induction
Vec CL1 CL2 CL3
B
Slug-3'UTR
WT
Mut363
RFU
NS
Vec 363
Vec 363
C
E-Cadherin fold of induction
Vec CL1 CL2 CL3
Vimentin fold of induction
Vec CL1 CL2 CL3
110-
E-Cad
1.00 1.08 1.37 1.60
54-
VIM
1.00 0.43 0.41 0.57
42-
Actin
Vec CL1 CL2 CL3
D
Rel. migrated cells
Con KD CL1 CL3
miR-363 fold of induction
Upper Lower
Con
CL1
KD
CL3
E
E-Cadherin fold of induction
Con
PCI-Slug
CL3
Vimentin fold of induction
Con
PCI-Slug
CL3
110-
E-Cad
1.00 0.74 0.33 0.07
54-
VIM
1.00 1.13 1.24 1.62
30-
Slug
42-
Actin
Con
PCI-Slug
CL3

Figure S4

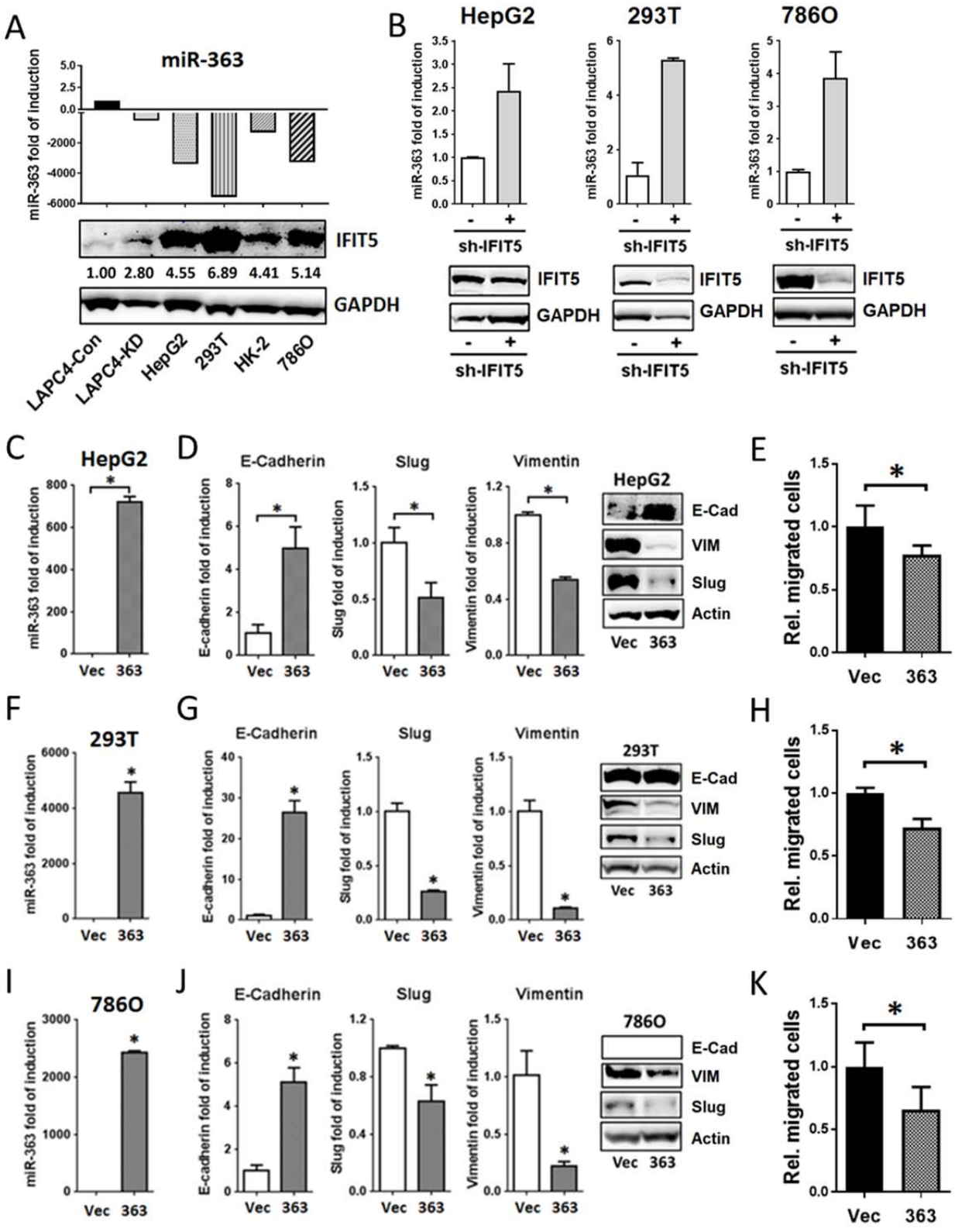
A
miR-363
miR-363 fold of induction
IFIT5
1.00 2.80 4.55 6.89 4.41 5.14
GAPDH
LAPC4-Con
LAPC4-KD
HepG2
293T
HK-2
786O
B
HepG2
293T
786O
sh-IFIT5
IFIT5
GAPDH
C
HepG2
Vec 363
D
E-Cadherin
Slug
Vimentin
E-cadherin fold of induction
Slug fold of induction
Vimentin fold of induction
E-Cad
VIM
Actin
E
Rel. migrated cells
F
293T
G
H
I
786O
J
K

Figure S5

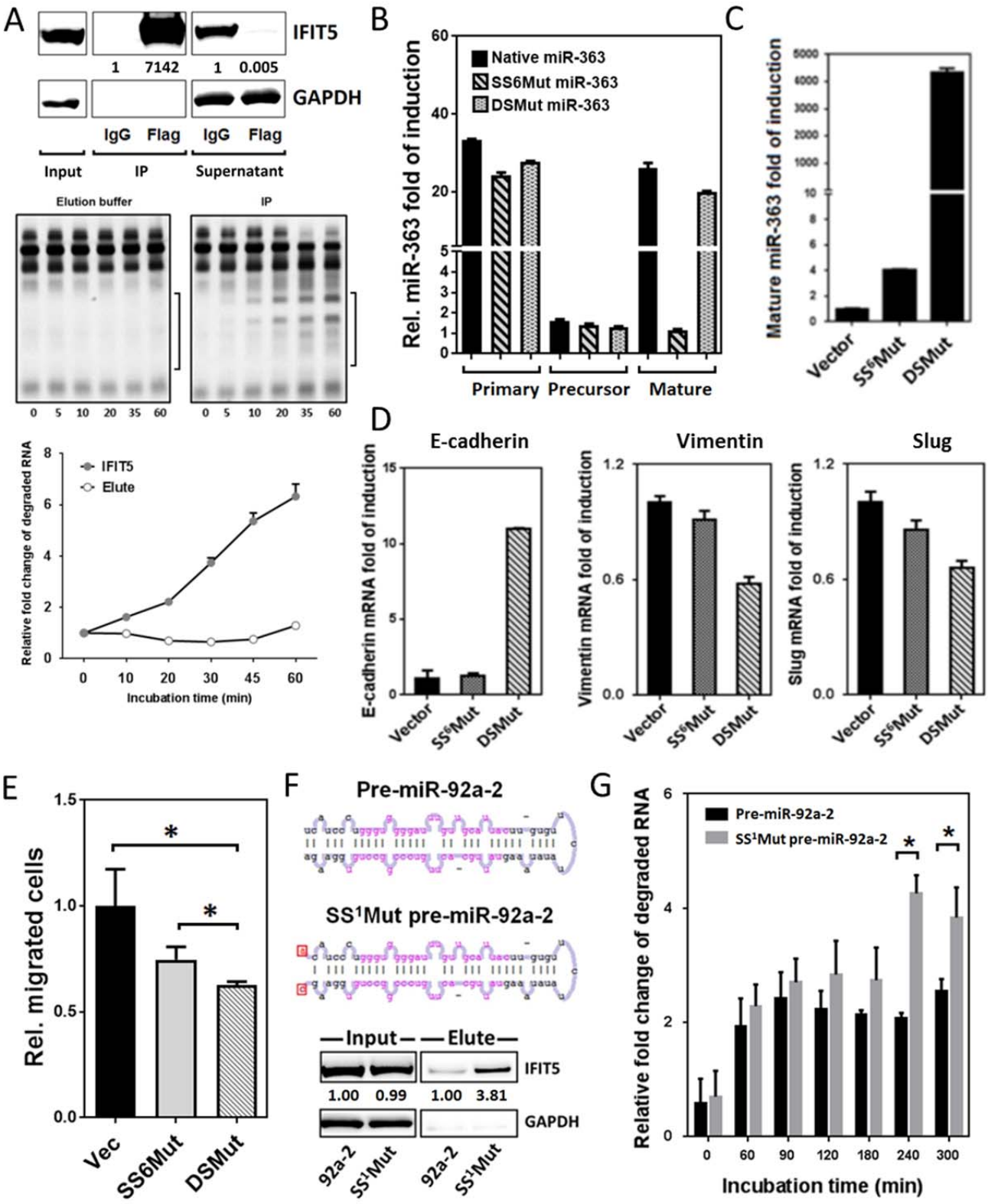
A
IFIT5
1 7142 1 0.005
GAPDH
IgG Flag IgG Flag
Input IP Supernatant
Elution buffer
IP
0 5 10 20 35 60 0 5 10 20 35 60
IFIT5
Elute
Relative fold change of degraded RNA
Incubation time (min)
B
Native miR-363
SS6Mut miR-363
DSMut miR-363
Rel. miR-363 fold of induction
Primary Precursor Mature
C
Mature miR-363 fold of induction
Vector SS6Mut DSMut
D
E-cadherin
Vimentin
Slug
E-cadherin mRNA fold of induction
Vimentin mRNA fold of induction
Slug mRNA fold of induction
Vector SS6Mut DSMut
E
Rel. migrated cells
Vec SS6Mut DSMut
F
Pre-miR-92a-2
SS1Mut pre-miR-92a-2
Input Elute
IFIT5
1.00 0.99 1.00 3.81
GAPDH
92a-2 SS1Mut 92a-2 SS1Mut
G
Pre-miR-92a-2
SS1Mut pre-miR-92a-2
Relative fold change of degraded RNA
Incubation time (min)

Figure S6

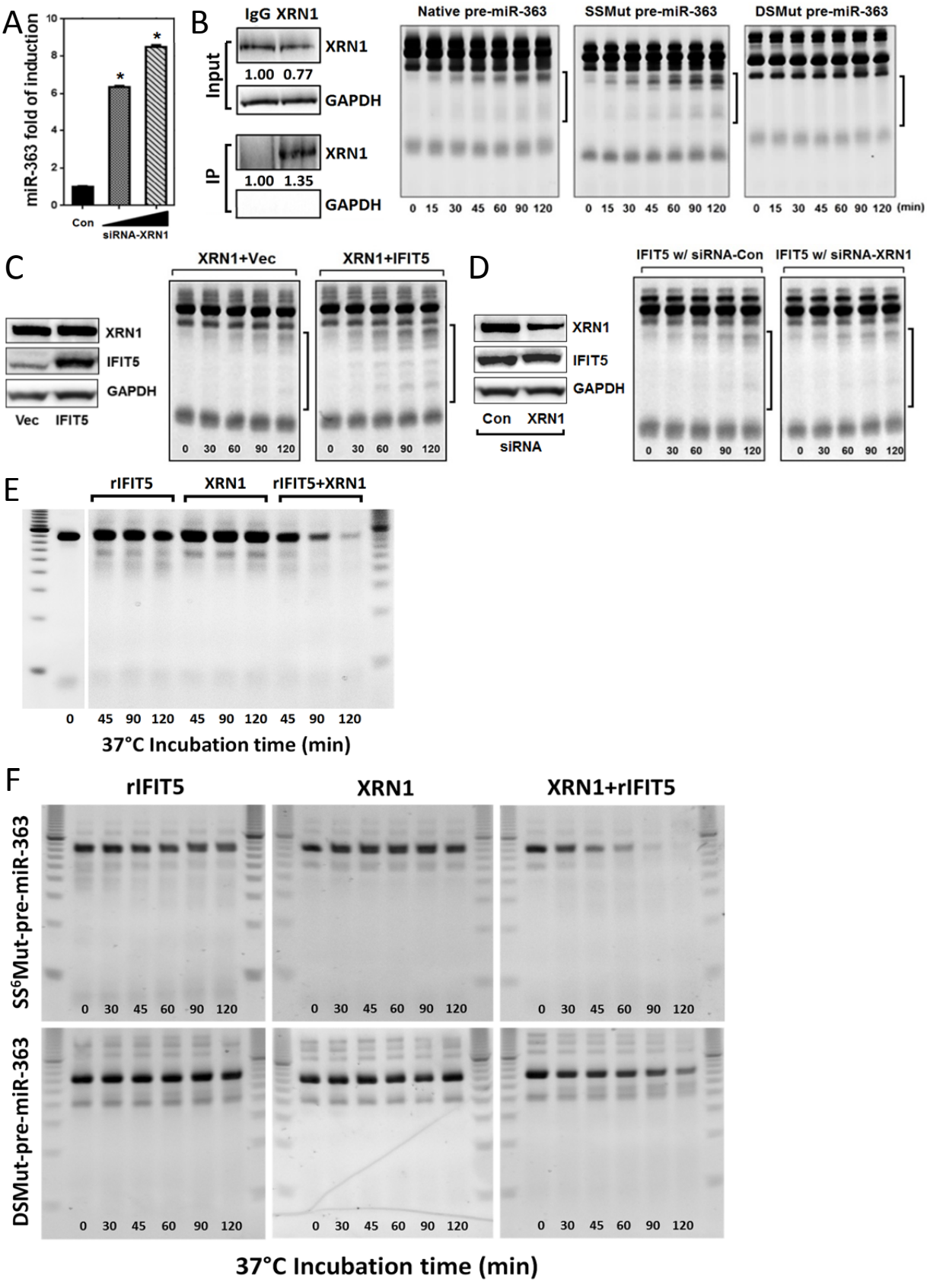
A
miR-363 fold of induction
Con
siRNA-XRN1
B
IgG XRN1
Input
XRN1
1.00 0.77
GAPDH
IP
XRN1
1.00 1.35
GAPDH
Native pre-miR-363
SSMut pre-miR-363
DSMut pre-miR-363
0 15 30 45 60 90 120 (min)
C
XRN1
IFIT5
GAPDH
Vec IFIT5
XRN1+Vec
XRN1+IFIT5
0 30 60 90 120
D
XRN1
IFIT5
GAPDH
Con XRN1
siRNA
IFIT5 w/ siRNA-Con
IFIT5 w/ siRNA-XRN1
0 30 60 90 120
E
rIFIT5
XRN1
rIFIT5+XRN1
0 45 90 120 45 90 120 45 90 120
37°C Incubation time (min)
F
rIFIT5
XRN1
XRN1+rIFIT5
SS6Mut-pre-miR-363
DSMut-pre-miR-363
0 30 45 60 90 120
37°C Incubation time (min)

Figure S7

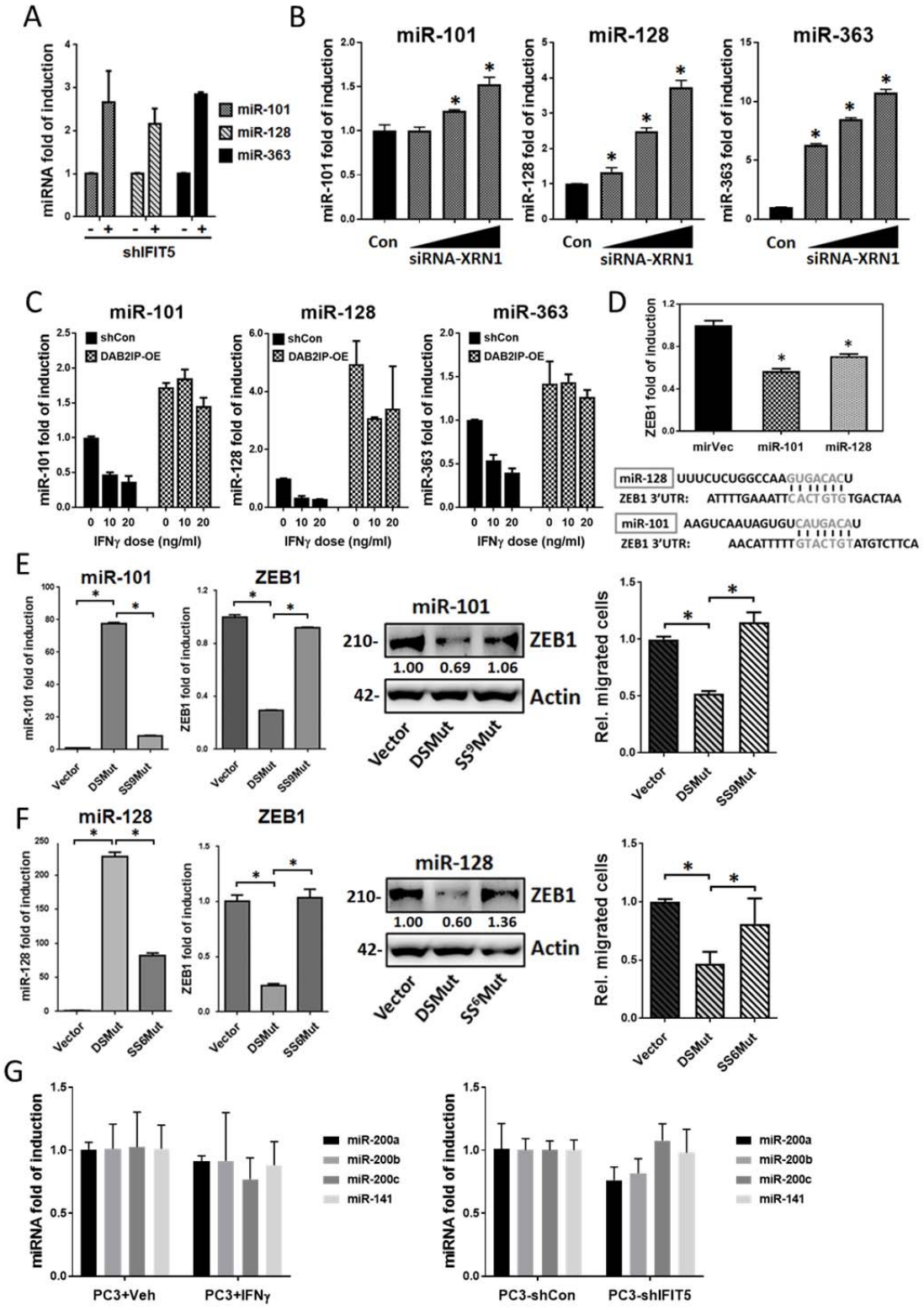
A
miRNA fold of induction
miR-101
miR-128
miR-363
shIFIT5
B
miR-101
miR-128
miR-363
miR-101 fold of induction
miR-128 fold of induction
miR-363 fold of induction
Con
siRNA-XRN1
C
miR-101
miR-128
miR-363
shCon
DAB2IP-OE
IFNγ dose (ng/ml)
D
ZEB1 fold of induction
mirVec
miR-101
miR-128
miR-128 UUUCUCUGGCCAAGUGACACU
ZEB1 3'UTR: ATTTTGAAATTCACTGTGTGACTAA
miR-101 AAGUCAAUAGUGUCAUGACAU
ZEB1 3'UTR: AACATTTTTGTACTGTATGTCTTCA
E
miR-101
ZEB1
miR-101 fold of induction
ZEB1 fold of induction
210-
42-
ZEB1
Actin
1.00 0.69 1.06
Vector
DSMut
SS9Mut
Rel. migrated cells
F
miR-128
ZEB1
miR-128 fold of induction
ZEB1 fold of induction
1.00 0.60 1.36
SS6Mut
G
miRNA fold of induction
miR-200a
miR-200b
miR-200c
miR-141
PC3+Veh
PC3+IFNγ
PC3-shCon
PC3-shIFIT5

Figure S8

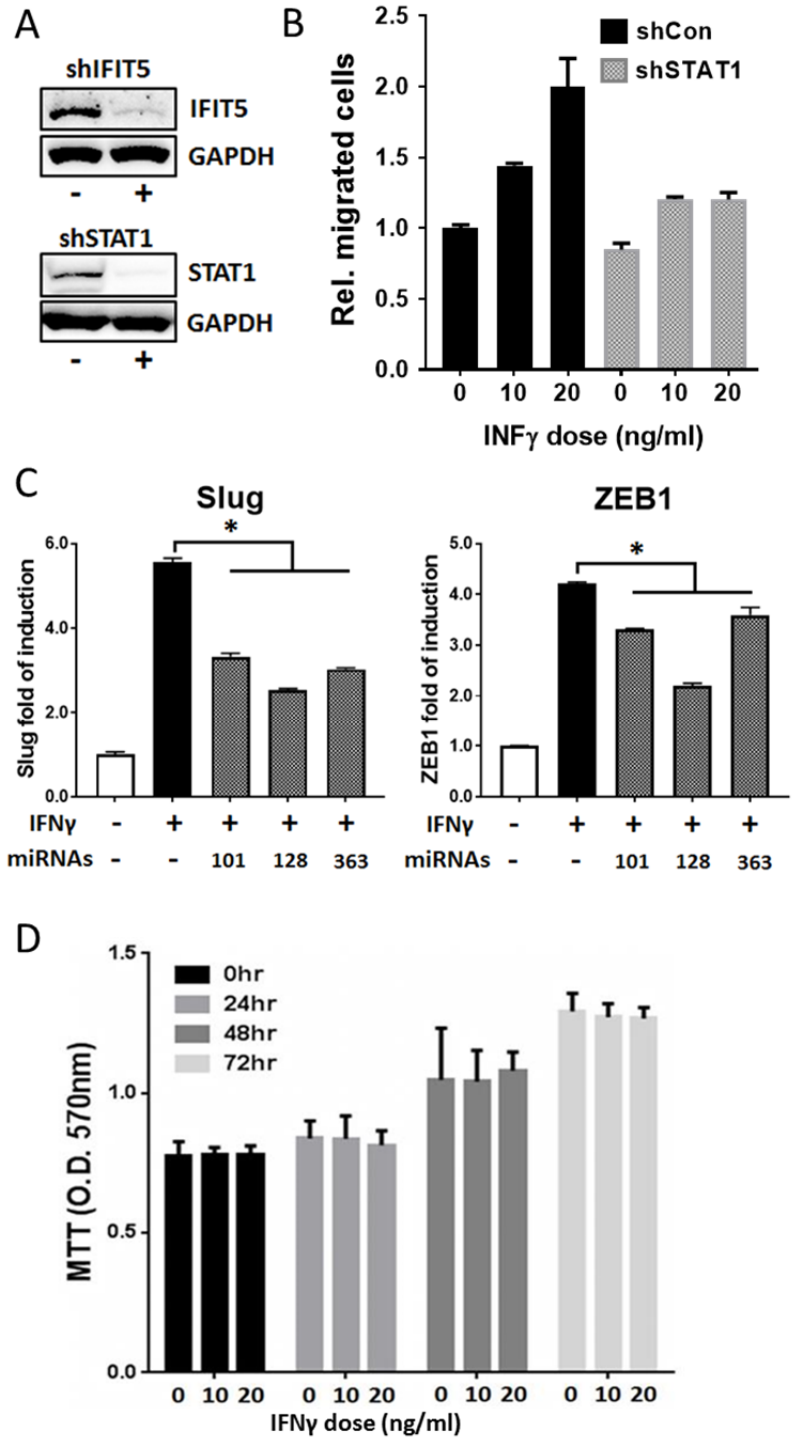
A
shIFIT5
IFIT5
GAPDH
- +
shSTAT1
STAT1
GAPDH
- +
B
shCon
shSTAT1
Rel. migrated cells
2.5
2.0
1.5
1.0
0.5
0.0
0 10 20 0 10 20
INFγ dose (ng/ml)
C
Slug
*
Slug fold of induction
6.0
4.0
2.0
0.0
IFNγ - + + + +
miRNAs - - 101 128 363
ZEB1
*
ZEB1 fold of induction
5.0
4.0
3.0
2.0
1.0
0.0
IFNγ - + + + +
miRNAs - - 101 128 363
D
0hr
24hr
48hr
72hr
MTT (O.D. 570nm)
1.5
1.0
0.5
0.0
0 10 20 0 10 20 0 10 20 0 10 20
IFNγ dose (ng/ml)

Figure S9

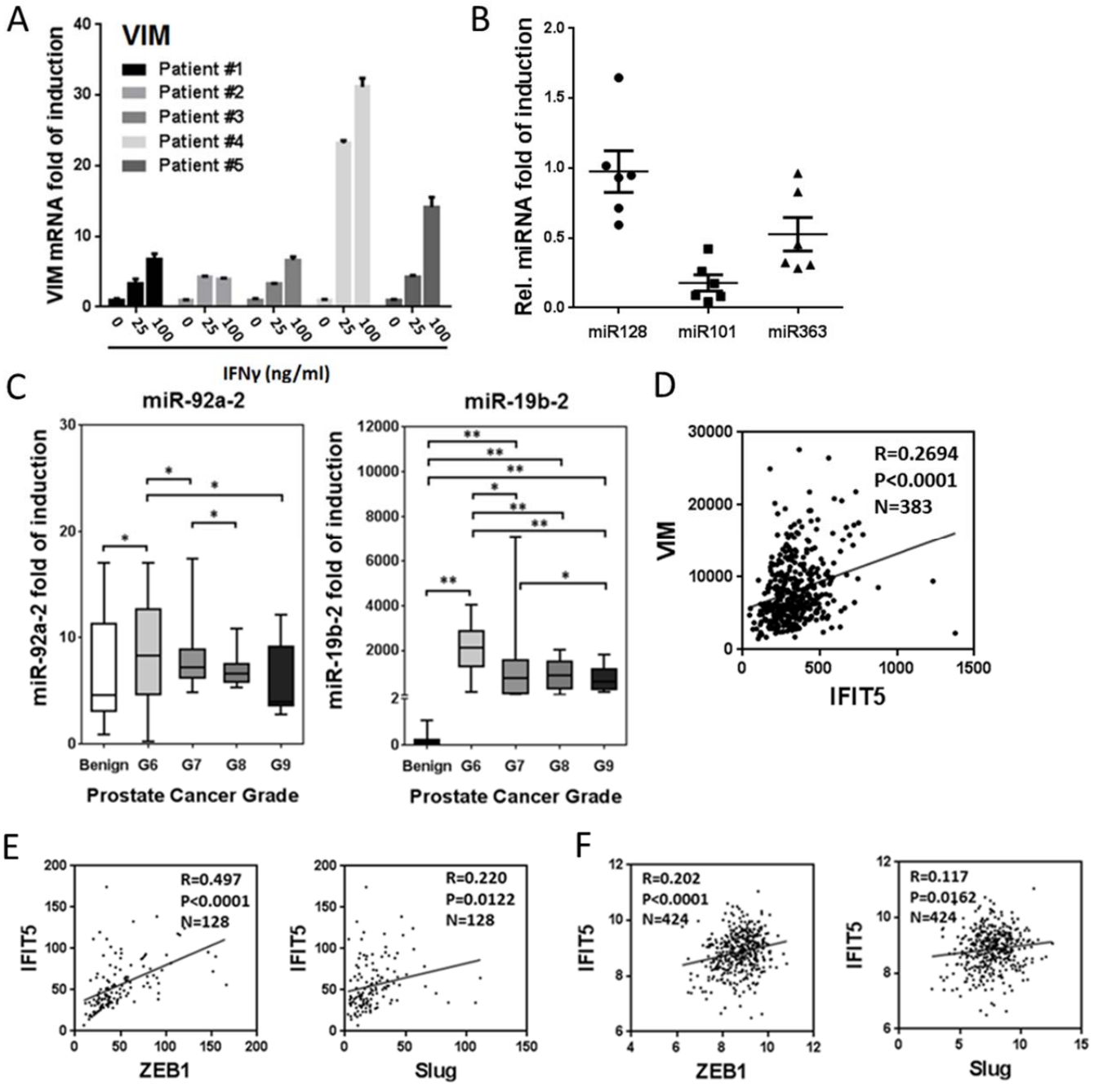
A
VIM
Patient #1
Patient #2
Patient #3
Patient #4
Patient #5
VIM mRNA fold of induction
IFNγ (ng/ml)
B
Rel. miRNA fold of induction
miR128
miR101
miR363
C
miR-92a-2
miR-19b-2
miR-92a-2 fold of induction
miR-19b-2 fold of induction
Benign G6 G7 G8 G9
Prostate Cancer Grade
D
R=0.2694
P<0.0001
N=383
VIM
IFIT5
E
R=0.497
P<0.0001
N=128
IFIT5
ZEB1
R=0.220
P=0.0122
N=128
Slug
F
R=0.202
P<0.0001
N=424
R=0.117
P=0.0162
N=424

SUPPLEMENTAL TABLES

Supplementary Table 1 List of protein candidates derived from Mass Spectrometry after using precursor miR-363 to pull down protein complex in a variety of cell line pairs (LAPC4, RWPE1 and C4-2) with or without DAB2IP expression

Cell line	DAB2IP-/DAB2IP+ Ratio	PSMs	Peptide Seqs	% Coverage	S. COUNTS		S. INDEX (MIC SIn)	
					DAB2IP+	DAB2IP-	DAB2IP+	DAB2IP-
IFIT5_HUMAN Interferon-induced protein with tetratricopeptide repeats 5 OS=Homo sapiens GN=IFIT5 PE=1 SV=1								
LAPC4	LAPC4-KD Only	20	12	22.40		20.00		1.57E-06
RWPE1	1.28	152	18	39.60	62.50	90.50	2.63E-05	3.37E-05
C4-2	C4-2Neo Only	3	2	3.70		2.99		3.82E-07
B9A067_HUMAN Mitochondrial inner membrane protein OS=Homo sapiens GN=IMMT PE=2 SV=2								
LAPC4	0.11	5	5	8.60	4.00	1.00	1.22E-07	1.39E-08
RWPE1	0.28	5	3	7.30	3.00	2.00	3.57E-07	9.96E-08
C4-2	0.17	58	31	36.80	49.05	7.85	6.29E-06	1.05E-06
SNUT1_HUMAN U4/U6.U5 tri-snRNP-associated protein 1 OS=Homo sapiens GN=SART1 PE=1 SV=1								
LAPC4	0.40	14	10	14.80	9.00	5.00	2.37E-07	9.43E-08
RWPE1	0.90	17	10	13.50	8.00	9.00	7.93E-07	7.11E-07
C4-2	0.31	12	7	11.90	9.00	3.00	5.98E-07	1.88E-07
ADT2_HUMAN ADP/ATP translocase 2 OS=Homo sapiens GN=SLC25A5 PE=1 SV=7								
LAPC4	0.32	24	9	28.90	12.96	10.97	5.78E-06	1.82E-06
RWPE1	0.38	13	8	28.20	6.50	5.50	6.89E-06	2.63E-06
C4-2	0.35	18	11	28.90	11.02	6.00	8.09E-06	2.87E-06
PARP1_HUMAN Poly [ADP-ribose] polymerase 1 OS=Homo sapiens GN=PARP1 PE=1 SV=4								
LAPC4	0.68	135	40	40.80	73.00	62.00	3.38E-06	2.31E-06
RWPE1	0.48	10	5	6.90	6.00	4.00	3.33E-07	1.61E-07
C4-2	0.62	22	22	23.10	16.00	6.00	1.04E-06	6.42E-07
XRCC5_HUMAN X-ray repair cross-complementing protein 5 OS=Homo sapiens GN=XRCC5 PE=1 SV=3								
LAPC4	0.36	29	16	22.80	18.98	9.99	6.73E-07	2.45E-07
RWPE1	0.17	35	17	24.60	26.99	9.00	3.54E-06	6.10E-07
C4-2	C4-2D2 Only	6	6	8.30	6.00		4.04E-07	
SFPQ_HUMAN Splicing factor, proline- and glutamine-rich OS=Homo sapiens GN=SFPQ PE=1 SV=2								
LAPC4	0.54	176	34	46.10	115.41	59.73	1.50E-05	8.10E-06
RWPE1	0.69	11	6	12.00	5.00	6.00	7.40E-07	5.14E-07
C4-2	0.58	27	14	19.80	15.96	10.99	2.57E-06	1.49E-06
ATPA_HUMAN ATP synthase subunit alpha, mitochondrial OS=Homo sapiens GN=ATP5A1 PE=1 SV=1								
LAPC4	0.32	20	12	22.80	13.76	5.88	8.06E-07	2.55E-07
RWPE1	0.94	28	12	29.30	13.78	13.79	1.75E-06	1.65E-06
C4-2	0.88	97	25	41.60	49.17	46.19	1.13E-05	1.00E-05
VDAC2_HUMAN Voltage-dependent anion-selective channel protein 2 OS=Homo sapiens GN=VDAC2 PE=1 SV=2								
LAPC4	0.05	12	8	32.50	10.87	0.99	1.36E-06	6.52E-08
RWPE1	0.52	7	4	15.20	3.96	2.97	2.34E-06	1.21E-06
C4-2	0.13	36	11	48.80	27.70	7.92	2.40E-05	3.20E-06
H4_HUMAN Histone H4 OS=Homo sapiens GN=HIST1H4A PE=1 SV=2								
LAPC4	LAPC4-Con Only	5	3	31.10	5.00		2.46E-06	
RWPE1	0.70	7	4	40.80	5.00	2.00	3.79E-06	2.64E-06
C4-2	0.08	7	3	31.10	6.00	1.00	1.14E-05	9.59E-07
CKAP4_HUMAN Cytoskeleton-associated protein 4 OS=Homo sapiens GN=CKAP4 PE=1 SV=2								
LAPC4	0.41	6	3	6.00	3.00	3.00	8.02E-08	3.28E-08
RWPE1	0.73	28	13	27.20	16.00	12.00	1.93E-06	1.41E-06
C4-2	0.33	23	14	28.10	15.97	6.97	1.77E-06	5.76E-07
ILF2_HUMAN Interleukin enhancer-binding factor 2 OS=Homo sapiens GN=ILF2 PE=1 SV=2								
LAPC4	1.25	303	21	48.20	140.00	163.00	1.31E-04	1.63E-04
RWPE1	1.09	142	20	57.70	70.00	73.00	5.76E-05	6.29E-05
C4-2	1.47	28	8	20.00	13.00	15.00	2.89E-06	4.27E-06
ACACA_HUMAN Acetyl-CoA carboxylase 1 OS=Homo sapiens GN=ACACA PE=1 SV=2								
LAPC4	1.19	47	28	14.40	25.88	20.92	1.95E-07	2.32E-07
RWPE1	1.31	820	115	58.50	174.15	259.86	2.10E-05	2.74E-05
C4-2	8.98	16	122	43.40	5.94	9.44	8.89E-08	7.98E-07
I3L1L3_HUMAN Myb-binding protein 1A (Fragment) OS=Homo sapiens GN=MYBBP1A PE=4 SV=1								
LAPC4	LAPC4-Con Only	22	19	17.90	22.00		6.31E-07	
RWPE1	0.29	3	2	1.80	2.00	1.00	5.15E-08	1.47E-08
C4-2	C4-2D2 Only	2	2	1.60	2.00		3.41E-08	

Supplemental Table 2. The incidence of lung metastasis, tumor nodule number and size in SCID mice receiving intravenous injection of IFIT5-knockdown PC3 cells (shIFIT5) pretreated with vehicle (Veh, PBS) or IFNγ (20ng/ml) for 48hrs, compared to PC3 cells transfected with control vector (shCon).

Group	shCon+Vehicle				shCon+IFNγ					shIFIT5+Vehicle	shIFIT5+IFNγ
Incidence (%)	4/14 (28.5%)				5/15 (33.3%)					1/15 (6.67%)	1/15 (6.67%)
Mouse #	1	2	3	4	1	2	3	4	5	1	1
Nodule numbers	2	2	10	6	15	12	35	20	52	9	1
Nodule/Lung (%)	0.42%	0.11%	2.88%	0.53%	0.77%	0.81%	7.02%	4.89%	24.72%	0.41%	0.14%

Supplemental Table 3. Primers designed for site-directed mutagenesis and PCR.

Primers used for site-directed mutagenesis:	
Insertion of T7 promoter upstream to pre-miR-363 sequence in pCMV-miR-363 expression plasmid	
Pre363+T7m1-Forward	5'-AAGTTCTGATATTTAGTCATTGTAATAATACGACTCAAATGATCTGTTTTGCTGTTGTCG-3'
Pre363+T7m1-Reverse	5'-CGACAACAGCAAAACAGATCATTTGAGTCGTATTATTACAATGACTAAATATCAGAACTT-3'
Pre363+T7m2-Forward	5'-TTAGTCATTGTAATAATACGACTCACTATAGGGCGAAATGATCTGTTTTGCTGTTGTCG-3'
Pre363+T7m2-Reverse	5'-CGACAACAGCAAAACAGATCATTTCGCCCTATAGTGAGTCGTATTATTACAATGACTAA-3'
Generating Mutant form of T7-pre-miR-363 DNA templates	
SDM_T7-363-DS-Forward	5'-GGCGAAATGATCTGTTTTGCGGTTTACGGGTGGATCAC-3'
SDM_T7-363-DS-Reverse	5'-GTGATCCACCCGTAAACCGCAAAACAGATCATTTCGCC-3'
SDM_T7-363-SS-Forward	5'-GGCGAAATGATCTGTTTTGCTCAAGTCGGGTGGATCAC-3'
SDM_T7-363-SS-Reverse	5'-GTGATCCACCCGACTTGAGCAAAACAGATCATTTCGCC-3'
Generating Mutant form of pre-miR-363 expression plasmids	
SDM_ pCMV363-DS-Forward	5'-TTGTAAAATGATCTGTTTTGCGGTTTACGGGTGGATCAC-3'
SDM_ pCMV363-DS-Reverse	5'-GTGATCCACCCGTAAACCGCAAAACAGATCATTTTACAA-3'
SDM-pCMV363-SS-Forward	5'-TTGTAAAATGATCTGTTTTGCTCAAGTCGGGTGGATCAC-3'
SDM-pCMV363-SS-Reverse	5'-GTGATCCACCCGACTTGAGCAAAACAGATCATTTTACAA-3'
Insertion of ApaI upstream to pre-miR-92a-2 sequence in pGEM-pre-92a-2 plasmid	
T7-Apa1-mut-Forwad	5'-ATTCGATTCTCTGGGCCCGCTTTCTTCCACAGGCCG-3'
T7-Apa1-mut-Reverse	5'-CGGCCTGTGGAAGAAAGCGGGCCCAGAGAATCGAAT-3'
Generating mutant miR-363 target site in siCHECK2-Slug 3'UTR	
SLUG-SDM-Forward	5'-CATTTTAATAATTTTTGAAAATTAATGGCTATATTTCCGGCAAATTTAAGAGGATTCTTAC-3'
SLUG-SDM-Reverse	5'-GTAAGAATCCTCTTAAATTTGCCGGAAATATAGCCATTAATTTTCAAAAATTATTAAAATG-3'
Insertion of Nhe1 into pre-miR-92a-2 sequence in pCMV-miR-363 plasmid	
92a-2 SDM Nhel-Forward	5'-TTCTATATAAAGTATTGCAGCTAGCCTTGTCCCGGCCTGTGGAA-3'
92a-2 SDM Nhel-Reverse	5'-TTCCACAGGCCGGGACAAGGCTAGCTGCAATACTTTATATAGAA-3'
Primers used for PCR:	
pre363wT7-Forward	5'-GTCATTGTAATAATACGACTCA-3'
pre363-Reverse	5'-GGTTTACAGATGGATACCG-3'
Pre92a-2-Forward	5'-GCCCATTCATCCCTGGGTGGGGATTTGT-3'
Pre92a-2-Reverse	5'-CTCCTTTCTTCCACAGGCCGGGACAAGT-3'
T7_pre92a-2-Forward	5'-TGTAATACGACTCACTATAGGGCGAAT-3'
T7_pre92a-2-Reverse	5'-TCATCCCTGGGTGGGGATTTGTTGCAT-3‘
SDM_T7-363-DS-Forward	5'-GGCGAAATGATCTGTTTTGCGGTTTACGGGTGGATCAC-3‘
SDM_T7-363-SS-Forward	5'-GGCGAAATGATCTGTTTTGCTCAAGTCGGGTGGATCAC-3'
Generating Mutant form of SN-A/C pre-miR-92a-2 DNA template	
X-92-5A-Fw	5'-TCTAGAACATCCCTGGGTGGGGATTTGT-3'
X-92-3C-Rv	5'-TCTAGAGCTTCCACAGGCCGGGACAAGT-3'

SUPPLEMENTAL INFORMATION

Plasmid constructions

Luciferase reporter plasmid siCHECK2-Slug3'UTR and psiCHECK2-Slug3'UTR-Mut^{363}

psiCHECK2-dual luciferase reporter construct (Promega) containing the wild type 3'UTR sequence of human SNAI2/Slug (psiCHECK2-Slug3'UTR-WT) was obtained from Dr. Jin-Tang Dong (Emory University). The Slug 3'UTR contains one putative target site of miR-363. We generated a psiCHECK2-Slug3'UTR-Mut^{363} plasmid by mutating the miR-363 target site using site-directed mutagenesis kit.

pCMV-miR-363 expression vector

The pCMV-miR-363 expression plasmid initially purchased from Origene contains both pre-miR-92a-2 and pre-miR-363 sequence. In order to isolate pre-miR-363 sequence, we generated a Nhel cut site in the 5'-end of pre-miR-92a-2 using site-directed mutagenesis and excised pre-miR-363 sequence by using both NheI and MluI enzyme then inserted into the pCMV-miRNA empty vector to generate miR-363 expression plasmid (Native pre-miR-363).

SSMut and DSMut precursor miRNA-expression plasmid constructs

We use native miRNA-expression plasmid as template to generate

We used Native miR-363 expressing plasmid (Origene) as a template to generate mutant pre-miR-363 with 5'-six nucleotides single stranded overhang (SSMut pre-miR-363) or double-stranded blunt end (DSMut pre-miR-363) constructs using site-directed mutagenesis kit.

We used Native miR-101 and miR-128 expressing plasmid (Genecopoeia) as templates to generate mutant pre-miR-101 with 6'-six nucleotides single stranded overhang (SS9Mut pre-miR-101) or double-stranded blunt end (DSMut pre-miR-101) constructs, as well as mutant pre-miR-128 with 6'-six nucleotides single stranded overhang (SS6Mut pre-miR-128) or double-stranded blunt end (DSMut pre-miR-128) constructs using site-directed mutagenesis.

Plasmid construct for in vitro transcription of Native and Mutant pre-miR-363 RNA molecules

A sequence of T7 promoter was inserted into the upstream of Native pre-miR-363 plasmid using two-step site-directed mutagenesis. This plasmid was further used as a template to generate T7-SSMut pre-miR-363 and T7-DSMut pre-miR-363 constructs using site-directed mutagenesis kit. Subsequently, these DNA templates were PCR amplified and cloned into pGEM-T_{Easy} vector (Promega). After DNA sequencing confirmation, they were subjected to *in vitro* transcription to generate Native, SSMut and DSMut pre-miR-363 RNA molecules.

Plasmid construct for in vitro transcription of pre-miR-92a-2 RNA molecules

The pre-miR-92a-2 sequence was PCR amplified and cloned into the downstream of T7 promoter in the pGEM-T_{Easy} vector. In order to generate a template for *in vitro* transcription, one ApaI site in addition to the internal ApaI (5 nucleotides downstream from the T7 promoter) was created from 4 nucleotides upstream from the pre-miR-92a-2 sequence. After ApaI cleavage and gel purification, the plasmid was re-ligated to generate T7-pre-miR-92a-2 DNA template that is used for *in vitro* transcription for produce pre-miR-92a-2 RNA molecules.

Recombinant IFIT5 protein preparation

pET28a-6XHis/3XFlag-tagged IFIT5 plasmid was transformed into BL21 competent cells, induced with 0.2 mM isopropyl β-D-thiogalactopyranoside (IPTG) and grown overnight at 22°C. Cells were resuspended in Buffer A (20 mM HEPES, pH 7.5, 150 mM NaCl, 5 mM imidazole, 1 mM Tris (2-carboxyethyl) phosphine (TCEP) and 10% glycerol), and lysed by sonication. After centrifugation, supernatant was applied to Ni-charged HiTrap FF column (GE Healthcare), and bound proteins were denatured by washing the column with Buffer A containing 6 M guanidine hydrochloride to remove bound RNA. The protein was then refolded and eluted in buffer A with 500 mM imidazole.

Mouse xenografts and pathologic examination

One million PC3 cells transfected with luciferase reporter gene were resuspended in 50 saline and injected intravenously through tail vein. Bioluminescence imaging (BLI) was carried out weekly to monitor tumor metastasis 6 weeks post-injection. At Week 8, lung from each group of mice were excised and paraffin-embedded for Hematoxylin and eosin (H&E) staining. All

animal protocols were approved by the Institutional Animal Care and Use Committee in UT Southwestern Medical Center.

Pathological examination for identifying the metastatic nodules at lung parenchyma was carried out by two pathologists. The number of metastatic nodules was determined from stitched picture of H&E slide from whole mount section using KEYENCE microscopy (BZ-x700, Itasca, IL). The size of metastatic nodules and the area of whole lung were measured using Nikon NIS-Elements BR software.